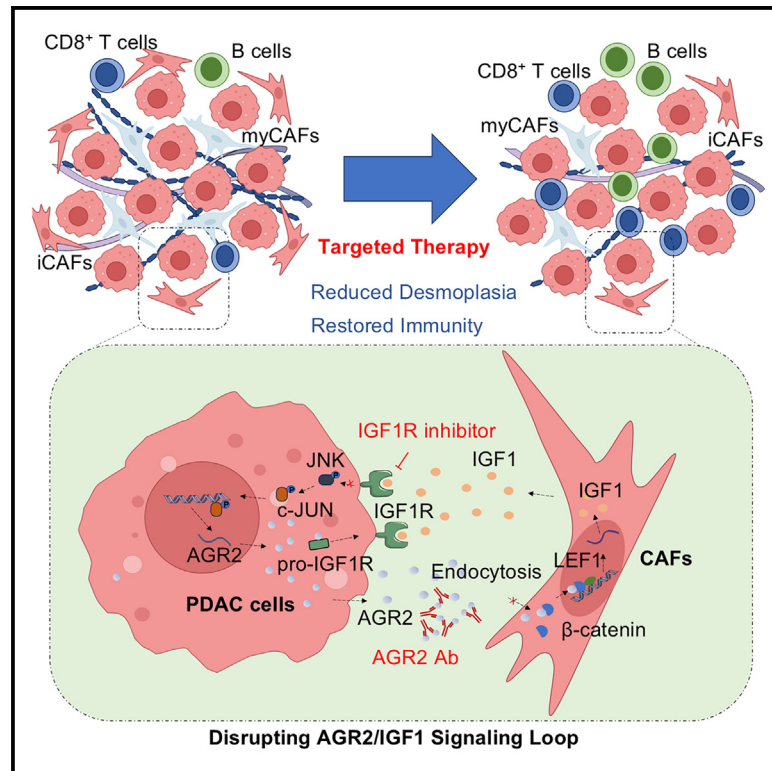


# Disrupting AGR2/IGF1 paracrine and reciprocal signaling for pancreatic cancer therapy

## Graphical abstract



## Authors

Hongzhen Li, Zhiheng Zhang, Zhao Shi, ..., Christoph W. Michalski, Shanshan Shen, Bo Kong

## Correspondence

shenss@nju.edu.cn (S.S.),  
bo.kong@med.uni-heidelberg.de (B.K.)

## In brief

PDAC interacts with stromal cells through secreted factors. Li et al. find that AGR2 secreted from tumor cells acts on CAFs to stimulate IGF1 secretion, which promotes the progression of PDAC. Targeting the AGR2/IGF1 loop restores anti-tumor immunity in PDAC, possessing potential therapeutic significance.

## Highlights

- Targeting AGR2/IGF1 disrupts harmful signaling in pancreatic cancer
- AGR2 and IGF1R co-inhibition reduces desmoplasia and immunosuppression
- Combined therapy restores anti-tumor immunity in preclinical PDAC models
- AGR2/IGF1 loop promotes PDAC progression via CAF activation and IGF1 secretion



## Article

# Disrupting AGR2/IGF1 paracrine and reciprocal signaling for pancreatic cancer therapy

Hongzhen Li,<sup>1,2,3,10</sup> Zhiheng Zhang,<sup>3,4,10</sup> Zhao Shi,<sup>1,2,5,10</sup> Siqi Zhou,<sup>1,2</sup> Shuang Nie,<sup>1,2</sup> Yuanyuan Yu,<sup>1,2,3</sup> Lingling Zhang,<sup>2,6</sup> Yifeng Sun,<sup>2,6</sup> Chao Fang,<sup>2,6</sup> Jingxiong Hu,<sup>2,6</sup> Yiqi Niu,<sup>2,6</sup> Kathleen Schuck,<sup>6</sup> Lei Wang,<sup>1</sup> Kuirong Jiang,<sup>7</sup> Zipeng Lu,<sup>7</sup> Christoph Kahlert,<sup>2</sup> Susanne Roth,<sup>2</sup> Martin Loos,<sup>2</sup> Ingrid Herr,<sup>2</sup> Yoshiaki Sunami,<sup>8</sup> Jörg Kleeff,<sup>8</sup> Helmut Friess,<sup>3</sup> Maximilian Reichert,<sup>9</sup> Zahra Dantes,<sup>9</sup> Xiaoping Zou,<sup>1</sup> Christoph W. Michalski,<sup>2</sup> Shanshan Shen,<sup>1,11,\*</sup> and Bo Kong<sup>2,11,12,\*</sup>

<sup>1</sup>Department of Gastroenterology, Nanjing Drum Tower Hospital, Affiliated Hospital of Medical School, Nanjing University, Nanjing, China

<sup>2</sup>Department of General, Visceral and Transplantation Surgery, University of Heidelberg, Heidelberg, Germany

<sup>3</sup>Department of Surgery, Klinikum Rechts der Isar, School of Medicine, Technical University of Munich (TUM), Munich, Germany

<sup>4</sup>Department of Hepatobiliary Surgery, Nanjing Drum Tower Hospital, Affiliated Hospital of Medical School, Nanjing University, Nanjing, China

<sup>5</sup>Department of Gastroenterology, Nanjing Drum Tower Hospital, Clinical College of Nanjing Medical University, Nanjing, Jiangsu Province, China

<sup>6</sup>Department of General and Visceral Surgery, Ulm University Hospital, Ulm, Germany

<sup>7</sup>Pancreas Center, The First Affiliated Hospital of Nanjing Medical University, Nanjing, China

<sup>8</sup>Department of Visceral, Vascular and Endocrine Surgery, Martin Luther University Halle-Wittenberg, Halle, Germany

<sup>9</sup>Department of Medicine II, Klinikum Rechts der Isar, Technische Universität München, Munich, Germany

<sup>10</sup>These authors contributed equally

<sup>11</sup>These authors contributed equally

<sup>12</sup>Lead contact

\*Correspondence: [shenss@nju.edu.cn](mailto:shenss@nju.edu.cn) (S.S.), [bo.kong@med.uni-heidelberg.de](mailto:bo.kong@med.uni-heidelberg.de) (B.K.)

<https://doi.org/10.1016/j.xcrm.2024.101927>

## SUMMARY

Pancreatic ductal adenocarcinoma (PDAC) is highly aggressive and characterized by pronounced desmoplasia. PDAC cells communicate with cancer-associated fibroblasts (CAFs) in a paracrine/reciprocal manner, substantially promoting tumor growth and desmoplastic responses. This study highlights the critical role of anterior gradient 2 (AGR2), an endoplasmic reticulum protein disulfide isomerase, secreted by PDAC cells to activate CAFs via the Wnt signaling pathway. Activated CAFs, in turn, secrete insulin-like growth factor 1 (IGF1), which enhances AGR2 expression and secretion in PDAC cells through the IGF1 receptor (IGF1R)/c-JUN axis. Within PDAC cells, AGR2 acts as a thioredoxin, aiding the folding and cell surface presentation of IGF1R, essential for PDAC's response to CAF-derived IGF1. This reciprocal AGR2/IGF1 signaling loop intensifies desmoplasia, immunosuppression, and tumorigenesis, creating a harmful feedback loop. Targeting both pathways disrupts this interaction, reduces desmoplasia, and restores anti-tumor immunity in preclinical models, offering a promising therapeutic strategy against PDAC.

## INTRODUCTION

Pancreatic ductal adenocarcinoma (PDAC) is a highly aggressive cancer characterized by abundant desmoplastic stroma, a dense network of extracellular matrix populated by cancer-associated fibroblasts (CAFs) and immune cells. Aberrant activation of CAFs occurs early in PDAC development.<sup>1</sup> Still, it remains unclear why only PDAC cells trigger such a strong desmoplastic reaction compared to other pancreatic cancers (e.g., acinar cell carcinoma). This suggests a unique role for PDAC cells as “organizers” that sculpt their surrounding stroma.<sup>2</sup> *In vitro* models using multivariate phosphoproteomics revealed that oncogenic Kras-driven PDAC cells activate CAFs via paracrine signaling through Sonic hedgehog (Shh), a potent growth and fibrosis factor. Activated CAFs then secrete insulin-like growth factor 1 (IGF1), promoting tumor cell proliferation and survival through the IGF1 receptor (IGF1R)/AKT pathway.<sup>3</sup> While initial preclinical

results were promising,<sup>4,5</sup> pharmaceutical inhibition of the Shh pathway (sonidegib) or IGF1R (ganitumab) in combination with gemcitabine failed to improve patient survival.<sup>6,7</sup> These findings suggest that targeting just one aspect of this complex crosstalk between tumor and CAFs is insufficient.

Three main CAF subtypes have been characterized: myofibroblastic CAFs (myCAFs), inflammatory CAFs (iCAFs), and antigen-presenting CAFs (apCAFs).<sup>8,9</sup> Driven by transforming growth factor  $\beta$  (TGF- $\beta$ ) and interleukin-1 (IL-1), myCAFs and iCAFs are believed to be derived from tissue-resident fibroblasts in the pancreas, with myCAFs being structure supportive and iCAFs being immune regulatory.<sup>10</sup> Lineage tracing revealed that mesothelial cells can acquire fibroblast-like features through IL-1 and TGF- $\beta$  signaling, becoming apCAFs. These apCAFs can convert naive CD4<sup>+</sup> T cells into regulatory T cells (Tregs) in an antigen-specific manner.<sup>11</sup> Given that iCAFs produce inflammatory mediators involved in tumorigenesis, it is accepted that iCAFs play an



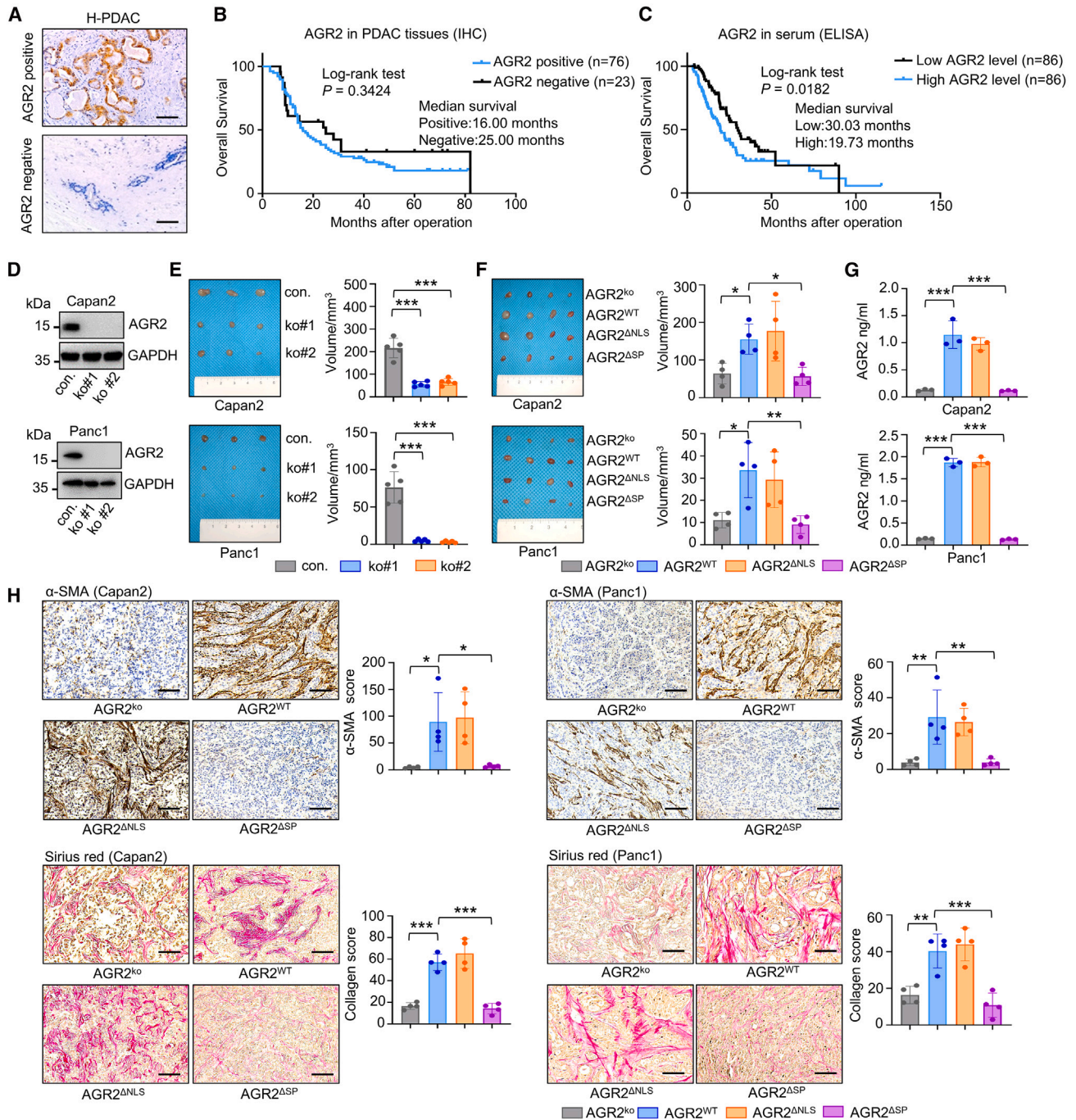


**Figure 1. Secreted AGR2 promotes pancreatic carcinogenesis by activating CAFs**

(A) Representative immunohistochemical (IHC) images demonstrate AGR2-positive and -negative PDAC tumors (scale bars: 50  $\mu$ m).

(B) Survival curves of patients categorized by AGR2 expression in PDAC tumor samples via IHC ( $n = 99$ ).

(C) Survival curves of patients stratified according to median AGR2 levels, measured by ELISA, in serum from individuals with PDAC ( $n = 172$ ).

(D) Western blot analyses of AGR2 expression in human PDAC cell lines (Capan2 and Panc1) following CRISPR-Cas9-mediated AGR2 knockout (performed in triplicate).

(E) Images and volumes of control versus AGR2-knockout subcutaneous xenografts derived from Capan2 and Panc1 cell lines in nude mice ( $n = 5$  per group). (F) Subcutaneous xenografts from AGR2-knockout Capan2 and Panc1 cells (AGR2<sup>KO</sup>), following re-expression of wild-type AGR2 (AGR2<sup>WT</sup>), AGR2 lacking a nuclear localization signal (AGR2<sup>ΔNLS</sup>), and AGR2 lacking a signal peptide (AGR2<sup>ΔSP</sup>) ( $n = 4$  per group).

(legend continued on next page)

oncogenic role, albeit this correlation has yet to be explicitly elucidated. As for myCAFs, it depends rather on the dominant type of collagen or specific marker that the given myCAFs express. Type I collagen-expressing myCAFs restrain PDAC progression,<sup>12</sup> while type III collagen-expressing ones promote metastasis.<sup>13</sup> Notably, a subset of myCAFs expressing leucine-rich repeat containing 15 (LRRC15) protein specifically promote tumor growth and immune exclusion.<sup>14,15</sup> Thus, it is appealing to specifically target those tumor-promoting CAFs while sparing the tumor-restraining ones.

Anterior gradient 2 (*AGR2*) encodes an oncogenic protein disulfide isomerase located in the endoplasmic reticulum (ER) and is known to be overexpressed in various cancers, including PDAC.<sup>16,17</sup> The function of *AGR2* is highly dependent on its cellular location. Within cells, *AGR2* serves as an adaptor protein facilitating the nuclear import of RNA polymerase II, consequently inhibiting p53 activation in the early stages of PDAC.<sup>18</sup> Specifically, *AGR2* is upregulated early in the transition from acinar-to-ductal metaplasia (ADM) to pancreatic intraepithelial neoplasia (PanIN). *AGR2* can also be secreted by various cancer types, leading to elevated levels of *AGR2* in bodily fluids.<sup>17,19,20</sup> Secreted *AGR2* activates RPTOR independent companion of MTOR complex 2 (RICTOR)/mTOR complex 2 (mTORC2) signaling in PDAC and Wnt signaling in colorectal cancer, promoting tumor progression through autocrine mechanisms.<sup>21,22</sup> Furthermore, *AGR2* enhances the migration, elongation, and proliferation of CAFs. This is supported by the uptake of secreted *AGR2* by CAFs through endocytosis, allowing it to bind directly to  $\beta$ -catenin through its dimer residue. This interaction increases the stability and nuclear accumulation of  $\beta$ -catenin in CAFs.<sup>23</sup> Additionally, *AGR2* stimulates CAF motility by activating RhoA-mediated cytoskeletal rearrangement.<sup>24</sup> Therefore, specifically targeting the paracrine functions of *AGR2* can potentially affect the behavior of CAFs in PDAC.

The aim of this study was to elucidate the signaling communication between PDAC and CAFs mediated by *AGR2* and IGF1 through paracrine and reciprocal interactions. To achieve this, we developed transgenic PDAC mouse models with either overexpression or deletion of *Agr2* in the pancreas and compared them with wild-type mice. Additionally, we analyzed human PDAC tissues along with clinicopathological data, transplanted tumor-derived PDAC cells subcutaneously into immunodeficient mice, and utilized both human and mouse organoid lines, as well as established PDAC cell lines. This comprehensive platform enabled us to investigate the desmoplastic reaction, immunosuppression, and tumorigenesis using a variety of biochemical, molecular biological, histological, and high-throughput assays.

## RESULTS

### Secreted *AGR2* promotes pancreatic carcinogenesis by activating CAFs

Immunohistochemical (IHC) analysis demonstrated that 77% (76 out of 99) of human PDAC specimens were positive for *AGR2* an-

tibodies (Figure 1A). Notably, *AGR2* staining was predominantly observed in PDAC cells rather than stromal cells. To confirm this finding, we analyzed publicly available single-cell RNA sequencing (scRNA-seq) data from PDAC samples (GEO: GSE155698),<sup>25</sup> which showed that *AGR2* expression is primarily derived from epithelial cells enriched for PDAC (Figure S1A). While *AGR2* expression levels in these samples were not associated with patient survival (Figure 1B), elevated serum *AGR2* levels and patient survival were observed, with patients with PDAC displaying elevated serum *AGR2* levels associated with reduced overall survival (Figure 1C,  $n = 172$ ). This suggests an oncogenic role for secreted *AGR2* in PDAC. To investigate this, we used CRISPR-Cas9 to knock out endogenous *AGR2* in four human PDAC cell lines (HPAC, Capan2, Panc1, and AsPC-1, Figure 1D; Figure S1B). *AGR2* knockout (*AGR2*<sup>KO</sup>) led to a significant reduction in tumor growth in corresponding xenograft models (Figure 1E; Figure S1C), consistent with previous studies.<sup>26</sup> We then rescued *AGR2* in knockout cells using vectors with synonymous mutations at the CRISPR-Cas9 target site. Wild-type *AGR2* (*AGR2*<sup>WT</sup>) and *AGR2* lacking a nuclear localization signal (*AGR2*<sup>ΔNLS</sup>) restored oncogenic activity, whereas *AGR2* with a signal peptide deletion (*AGR2*<sup>ΔSP</sup>), impairing secretion, did not (Figure 1F; Figure S1D). Enzyme-linked immunosorbent assay (ELISA) confirmed the secretion defect in *AGR2*<sup>ΔSP</sup> (Figure 1G; Figure S1E). Xenograft tumors with effective *AGR2* secretion (*AGR2*<sup>WT</sup> and *AGR2*<sup>ΔNLS</sup>) showed higher CAF infiltration and collagen deposition compared to those with deficient (*AGR2*<sup>ΔSP</sup>) or absent (*AGR2*<sup>KO</sup>) *AGR2* secretion, as determined by IHC staining and western blot analysis of murine pancreatic tissue (Figure 1H; Figures S1F and S1G). Despite these differences, tumor proliferation rates remained unchanged. These findings suggest that secreted *AGR2* activates CAFs, contributing to tumor maintenance.

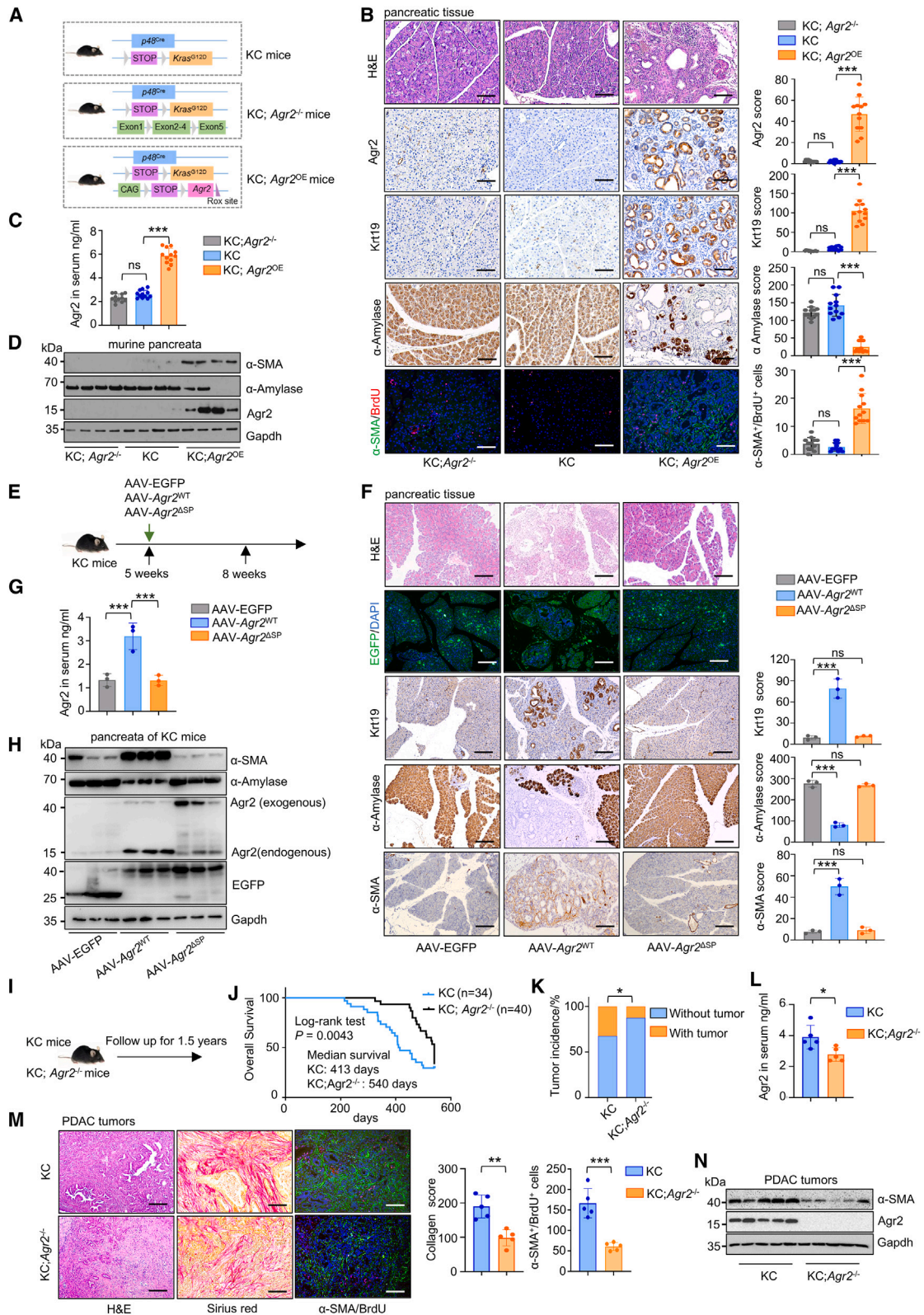
### *Agr2* secretion correlates with the desmoplastic reaction in genetic mouse models of PDAC

We engineered a transgenic mouse model that overexpresses *Agr2*. A FLAG-tagged *Agr2* cDNA construct, flanked by loxP-STOP-loxP sequences, was inserted into the *Rosa26* locus of the mouse genome, resulting in the *LSL-Rosa*<sup>CAG-*Agr2*</sup> model. Activation in pancreatic epithelial cells via p48<sup>Cre</sup> led to *Agr2* overexpression (*Agr2*<sup>OE</sup>). Additionally, we developed mice with floxed *Agr2* alleles for Cre-dependent knockout (*Agr2*<sup>-/-</sup>), as previously described.<sup>18</sup> We established the following three mouse models: KC (*p48*<sup>Cre/+</sup>; *LSL-Kras*<sup>G12D/+</sup>), KC; *Agr2*<sup>OE</sup> (*p48*<sup>Cre/+</sup>; *LSL-Kras*<sup>G12D/+</sup>; *LSL-Rosa*<sup>CAG-*Agr2*</sup>), and KC; *Agr2*<sup>-/-</sup> (*p48*<sup>Cre/+</sup>; *LSL-Kras*<sup>G12D/+</sup>; *Agr2*<sup>flox/flox</sup>) for comparison (Figure 2A).

At 8 weeks, KC; *Agr2*<sup>OE</sup> mice showed ADM and PanIN lesions (Figure 2B; Figures S2A and S2B). These lesions were associated with proliferative CAFs, unlike in KC and KC; *Agr2*<sup>-/-</sup> mice. KC; *Agr2*<sup>OE</sup> mice had significantly higher serum *Agr2* levels compared to KC and KC; *Agr2*<sup>-/-</sup> mice (Figure 2C).

(G) ELISA analyses of the supernatant from *AGR2*-knockout Capan2 and Panc1 cells re-expressing *AGR2*<sup>WT</sup>, *AGR2*<sup>ΔNLS</sup>, and *AGR2*<sup>ΔSP</sup> (performed in triplicate). (H) Representative IHC images and quantification of alpha-smooth muscle actin ( $\alpha$ -SMA) staining score and collagen score within xenograft tumors across the four groups ( $n = 4$  per group, scale bars: 50  $\mu$ m).

Statistical significance was determined using a log rank test for (B) and (C) and a one-way ANOVA with multiple comparisons test for (E) through (H). Data are presented as mean  $\pm$  standard deviation (SD). Significance levels are indicated as \* $p < 0.05$ , \*\* $p < 0.01$ , \*\*\* $p < 0.001$ .



(legend on next page)

Overexpression of *Agr2* resulted in elevated pancreatic levels of *Agr2* and alpha-smooth muscle actin ( $\alpha$ -SMA) and reduced  $\alpha$ -amylase, indicating fibrosis and compromised exocrine function (Figure 2D; compare Figure 2B). This condition led to severe diarrhea and weight loss in KC; *Agr2*<sup>OE</sup> mice, with a median survival of 59.5 days due to exocrine insufficiency. None of these mice developed invasive PDACs. In the absence of *Kras*<sup>G12D</sup>, *Agr2*<sup>OE</sup> did not induce any observable physiological changes in the pancreas, as confirmed by histologic analysis and staining for the endocrine marker insulin and the exocrine markers keratin 19 and  $\alpha$ -amylase (Figure S2C).

To provide *in vivo* evidence of the oncogenic potential of the secreted form of *Agr2*, we used an adeno-associated virus (AAV)-mediated transgene delivery system. Specifically, AAV particles encoding murine *Agr2*<sup>WT</sup> or *Agr2*<sup>ASP</sup> fused with enhanced green fluorescent protein (EGFP) were injected into the pancreata of 5-week-old KC mice (Figure 2E). All mice were sacrificed for analysis at 8 weeks of age. In contrast to KC mice injected with control AAV particles (EGFP), those injected with AAV-*Agr2*<sup>WT</sup> displayed marked histological changes, including proliferative ADM and PanIN lesions accompanied by desmoplastic reactions and a reduction in intact acinar cells labeled by  $\alpha$ -amylase (Figure 2F; Figure S2D). Notably, these effects were absent in mice injected with AAV-*Agr2*<sup>ASP</sup> particles. Correspondingly, serum *Agr2* levels were elevated in KC mice treated with AAV-*Agr2*<sup>WT</sup> compared to controls and AAV-*Agr2*<sup>ASP</sup> (Figure 2G). Due to the expansion of neoplastic ADM/PanIN lesions, we observed diluted EGFP signals alongside exogenous *Agr2*, as well as increased endogenous *Agr2* expression, confirmed by western blot analysis of AAV-*Agr2*<sup>WT</sup> pancreata (Figure 2H).

Since the phenotypes of KC and KC; *Agr2*<sup>-/-</sup> pancreata were indistinguishable at 8 weeks, we aged cohorts of KC; *Agr2*<sup>-/-</sup> ( $n = 40$ ) and KC ( $n = 34$ ) mice for up to 1.5 years to examine the long-term impact of *Agr2* on pancreatic carcinogenesis (Figure 2I). Long-term analysis showed that KC; *Agr2*<sup>-/-</sup> mice had a median survival of 540 days, longer than the 413 days of KC mice ( $n = 34$ , Figure 2J). The incidence of PDAC in KC; *Agr2*<sup>-/-</sup> mice

was 12.5% (5/40), significantly lower than 32.4% (11/34) in KC mice (Figure 2K). Lower serum *Agr2* levels were observed in KC; *Agr2*<sup>-/-</sup> mice compared to KC mice with PDAC (Figure 2L). PDAC tumors in KC; *Agr2*<sup>-/-</sup> mice had less CAF infiltration and collagen deposition compared to KC mice, as shown by immunofluorescence and Sirius red staining and western blot analysis of murine pancreata (Figures 2M and 2N). These findings indicate that secreted *Agr2* contributes to CAF activation and desmoplastic reaction of PDAC.

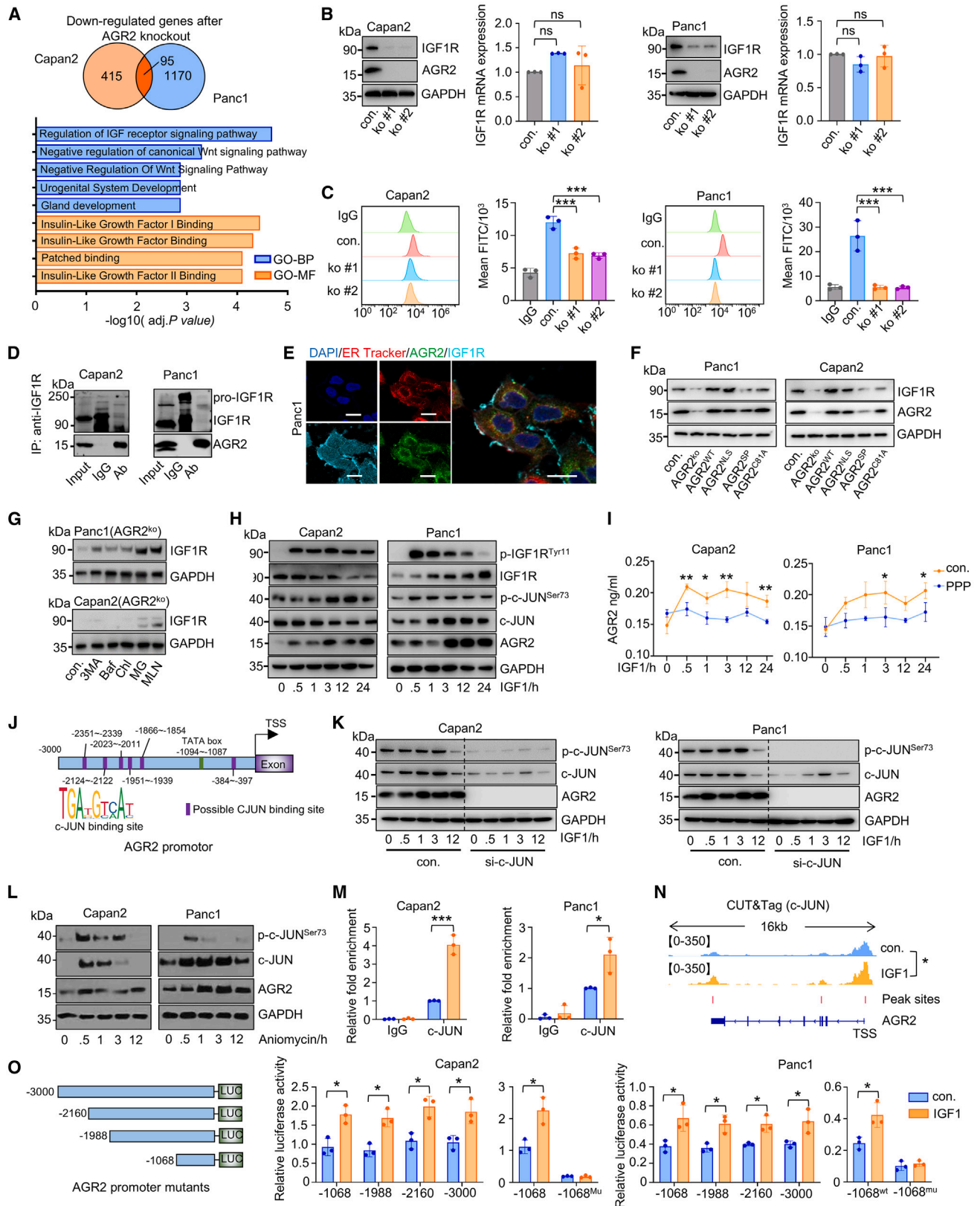
### IGF1 promotes AGR2 secretion and enhances IGF1R presentation on the cell surface

To elucidate the mechanism, we performed RNA sequencing (RNA-seq) on AGR2<sup>KO</sup> Capan2 and Panc1 cells. We found 510 and 1,265 differentially expressed genes (DEGs) in these cells. Gene set enrichment analysis highlighted “regulation of the IGF receptor signaling pathway” and “insulin-like growth factor I binding” as significantly enriched terms (Figure 3A). Western blot analysis revealed that AGR2<sup>KO</sup> reduced IGF1R protein levels without affecting mRNA levels in PDAC cell lines (Figure 3B). Flow cytometry and western blot analysis of the membrane fraction confirmed reduced surface IGF1R after AGR2 depletion (Figure 3C; Figure S3A).

AGR2, a thioredoxin-like protein, involved in protein folding through disulfide bond formation,<sup>27,28</sup> may potentially facilitate IGF1R folding by interaction with its cysteine-rich region (IGF1R residues 223–274).<sup>29</sup> Co-immunoprecipitation (coIP) assays demonstrated that AGR2 interacts with the precursor form of IGF1R (Figure 3D). Confocal microscopy revealed their co-localization in the ER (Figure 3E). Introducing AGR2 wild type or mutants into AGR2<sup>KO</sup> cells revealed that only AGR2<sup>WT</sup> and AGR2<sup>ΔNLS</sup> restored IGF1R levels, while AGR2<sup>ΔSP</sup> or a mutated active site (AGR2<sup>C81A</sup>) did not (Figure 3F). This suggests that AGR2 supports IGF1R folding via its thioredoxin activity. AGR2<sup>KO</sup> caused misfolded IGF1R accumulation, triggering ER stress and ER-associated degradation. Proteasomal (MG132 and MLN4924), but not lysosomal (3-methyladenine [3-MA], bafilomycin, and chloroquine), degradation inhibitors restored IGF1R

### Figure 2. *Agr2* secretion correlates with desmoplastic reaction in genetic mouse models of PDAC

- (A) Schematic illustration of the genotypes for KC mice, KC; *Agr2*<sup>-/-</sup> mice, and KC; *Agr2*<sup>OE</sup> mice.  
 (B) Representative hematoxylin and eosin (H&E), *Agr2*, Krt19, and  $\alpha$ -amylase-stained sections, along with  $\alpha$ -SMA/BrdU-stained immunofluorescence images of pancreata from KC, KC; *Agr2*<sup>-/-</sup>, and KC; *Agr2*<sup>OE</sup> mice (scale bars: 50  $\mu$ m;  $n = 12$  mice per group). The images were scored and thereby quantified (right).  
 (C) ELISA analysis of *Agr2* levels in the serum of 8-week-old KC, KC; *Agr2*<sup>-/-</sup> and KC; *Agr2*<sup>OE</sup> mice ( $n = 12$  mice per group).  
 (D) Western blot analysis of  $\alpha$ -SMA,  $\alpha$ -amylase, and *Agr2* expression in the pancreata of KC, KC; *Agr2*<sup>-/-</sup>, and KC; *Agr2*<sup>OE</sup> mice ( $n = 4$  mice per group).  
 (E) Schematic representation of KC mice injected with AAV-EGFP, AAV-*Agr2*<sup>WT</sup>, and AAV-*Agr2*<sup>ASP</sup> particles.  
 (F) Representative images of H&E staining, EGFP immunofluorescence, and IHC for Krt19,  $\alpha$ -amylase, and  $\alpha$ -SMA in the pancreata of KC mice injected with AAV-EGFP, AAV-*Agr2*<sup>WT</sup>, and AAV-*Agr2*<sup>ASP</sup> particles (scale bars: 50  $\mu$ m;  $n = 3$  mice per group). The images were scored and thereby quantified (right).  
 (G) ELISA analysis of *Agr2* levels in the serum of KC mice injected with AAV-EGFP, AAV-*Agr2*<sup>WT</sup>, and AAV-*Agr2*<sup>ASP</sup> particles.  
 (H) Western blot analysis of  $\alpha$ -SMA,  $\alpha$ -amylase, *Agr2*, and EGFP expression in the pancreata of KC mice injected with AAV-EGFP, AAV-*Agr2*<sup>WT</sup>, and AAV-*Agr2*<sup>ASP</sup> particles.  
 (I and J) Schematic representation and survival curves for KC and KC; *Agr2*<sup>-/-</sup> mice over a 1.5-year follow-up period.  
 (K) PDAC incidence in KC (11/34, 32.4%) versus KC; *Agr2*<sup>-/-</sup> mice (5/40, 12.5%).  
 (L) ELISA analysis of *Agr2* levels in the serum of KC and KC; *Agr2*<sup>-/-</sup> mice with PDAC ( $n = 5$  mice per group).  
 (M) Representative H&E-stained sections showing PDAC tumors in KC and KC; *Agr2*<sup>-/-</sup> mice; Sirius red-stained sections showing collagen distribution in tumors;  $\alpha$ -SMA/BrdU-stained immunofluorescence images depicting proliferative  $\alpha$ -SMA-positive cells in tumors (scale bars: 50  $\mu$ m;  $n = 5$  mice per group).  
 (N) Western blot analysis of  $\alpha$ -SMA and *Agr2* expression in tumors from KC mice and KC; *Agr2*<sup>-/-</sup> mice ( $n = 5$  mice per group).  
 Statistical significance for (B), (C), (G), and (F) was assessed using a one-way ANOVA with multiple comparisons test, (J) with a log rank test, (K) with a chi-squared test, and (L) and (M) with two-tailed, unpaired Student's *t* tests. Data are presented as mean  $\pm$  SD. Significance is denoted as \* $p < 0.05$ , \*\* $p < 0.01$ , \*\*\* $p < 0.001$ . “ns” indicates no significance.



(legend on next page)

levels (Figure 3G), highlighting the role of AGR2 in IGF1R folding and membrane presentation.

IGF1 treatment increased AGR2 at mRNA and protein levels and its secretion (Figures 3H and 3I; Figure S3B). Inhibiting IGF1R with picropodophyllin (PPP) partially reduced IGF1's effect on AGR2 expression and secretion (Figure S3C). IGF1 activated IGF1R and the non-canonical c-JUN pathway, as shown by phosphorylation at Tyr1135 and Ser73, respectively.

Analysis of the AGR2 promoter region revealed multiple c-JUN-binding sites, suggesting that AGR2 expression could be regulated through the c-JUN pathway (Figure 3J). Indeed, c-JUN knockdown reduced basal AGR2 levels and completely inhibited IGF1-induced AGR2 expression (Figure 3K). Moreover, stimulation of the c-Jun N-terminal kinase pathway, upstream of c-JUN, with anisomycin, replicated the IGF1-induced AGR2 expression (Figure 3L). In contrast, wortmannin inhibition of the phosphatidylinositol 3-kinase pathway, downstream of IGF1R, did not affect AGR2 levels (Figure S3D). These data highlight the specific regulatory role of c-JUN in mediating AGR2 expression in response to IGF1 signaling in PDAC cells.

Chromatin immunoprecipitation followed by quantitative PCR analysis revealed that c-JUN binds to the AGR2 promoter, and this binding is enhanced by IGF1 treatment (Figure 3M). This interaction was confirmed using cleavage under targets and tagmentation assays, which targeted c-JUN in Panc1 cells. Regardless of IGF1 treatment, a distinct c-JUN occupancy peak was observed upstream of the transcription start site at the AGR2 locus (Figure 3N). To determine the functional relevance of this binding site, we constructed several AGR2 promoter mutants and used luciferase reporter assays (Figure 3O). These assays pinpointed the critical role of the c-JUN-binding site located within the  $-1,068$  to  $+12$  bp region relative to the AGR2 promoter. Specifically, deletion within the  $-384$  to  $-397$  region

significantly impaired promoter activity, underscoring the functional importance of this c-JUN-binding site.

Our analyses demonstrate that IGF1 promotes AGR2 expression and secretion through the IGF1R/c-JUN signaling pathway in PDAC cells. AGR2, in turn, interacts with the precursor form of IGF1R in the ER and facilitates its membrane presentation, establishing a feedback loop within PDAC cells.

### Secreted AGR2 promotes IGF1 production from CAFs via the Wnt/ $\beta$ -catenin pathway

CAFs are a primary source of IGF1 in PDAC,<sup>3</sup> and AGR2 is known to activate fibroblasts.<sup>19,24,30</sup> We hypothesized that PDAC-secreted AGR2 induces IGF1 production in CAFs. Our data confirm that PDAC-derived CAFs produce IGF1 *in vitro* (Figure 4A). Co-culturing CAFs with patient-derived PDAC organoids significantly increased IGF1 secretion, as shown by elevated IGF1 mRNA levels and ELISA measurements of IGF1 in the culture supernatant (Figure 4B). This activated the IGF1R signaling pathway in PDAC cells, evidenced by western blot analysis (Figure S4A).

The enhanced IGF1 production was reduced by using a specific AGR2-neutralizing antibody (Figure 4B). To explore this further, CAFs were co-cultured with AGR2<sup>KO</sup> PDAC cells constituted with AGR2<sup>WT</sup>, AGR2<sup>ANLS</sup>, or AGR2<sup>ASP</sup>. IGF1 expression in CAFs increased when co-cultured with PDAC cells expressing AGR2<sup>WT</sup> or AGR2<sup>ANLS</sup>, indicating the importance of AGR2 secretion. Co-culture with AGR2<sup>KO</sup> or AGR2<sup>ASP</sup> cells did not affect IGF1 levels, which were reflected in the IGF1R signaling pathway of PDAC cells, including phosphorylated IGF1R and c-JUN levels (Figure 4C). Interestingly, we observed that co-culture with AGR2-secreting PDAC cells (AGR2<sup>WT</sup> or AGR2<sup>ANLS</sup>) consistently elevated iCAF marker expression, including IL-6, complement factor D (CFD), and C-C motif chemokine ligand 2 (CCL2).

### Figure 3. IGF1 promotes the secretion of AGR2, which in turn enhances the presentation of the IGF1R on the cell surface

(A) The Venn diagram of the upper panel illustrates the count of genes down-regulated in Capan2 and Panc1 cells post AGR2 knockout. The Gene Ontology (GO) analysis of the lower panel identifies enriched biological processes, notably "regulation of IGF receptor signaling pathway" at transcriptional levels, after AGR2 knockout in these cell lines.

(B) Western blot and quantitative reverse-transcription PCR (qRT-PCR) analyses assess IGF1R and AGR2 expression in Capan2 and Panc1 cells following AGR2 knockout via the CRISPR-Cas9 system (performed in triplicate).

(C) Flow cytometry (FACS) quantifies cell membrane surface expression of IGF1R in Capan2 and Panc1 cells after AGR2 knockout (performed in triplicate).

(D) Co-immunoprecipitation assays reveal AGR2's interaction with pro-IGF1R in Capan2 and Panc1 cells (performed in triplicate).

(E) Immunofluorescence imaging displays AGR2 and IGF1R distribution and ER labeling in Panc1 cells (scale bars: 50  $\mu$ m).

(F) Western blot analysis of IGF1R and AGR2 in Panc1 and Capan2 cells with controls (original cell lines), AGR2-knockout (AGR2<sup>KO</sup>) post-expression of AGR2<sup>WT</sup>, AGR2<sup>ANLS</sup>, AGR2<sup>ASP</sup>, and AGR2<sup>C81A</sup> mutation (performed in triplicate).

(G) Western blot analysis of IGF1R expression in AGR2 in Panc1 and Capan2 cells with AGR2 knockout (KO) treated with 3-methyladenine (3-MA) (15 mM), bafilomycin A1 (30 nM), chloroquine (20 mM), MLN4929 (1 mM), or MG132 (5 mM) for 12 h (performed in triplicate).

(H) Western blot analysis of IGF1R, phosphorylated IGF1R, c-JUN, phosphorylated c-JUN, and AGR2 following 12 h of serum starvation and subsequent IGF1 stimulation (50 ng/mL, performed in triplicate).

(I) ELISA measures AGR2 secretion after serum starvation and treatment with PPP (1  $\mu$ M) and IGF1 (50 ng/mL) over time (performed in triplicate).

(J) Identification of potential c-JUN-binding sites within the AGR2 promoter region.

(K) Western blot analysis of c-JUN, phosphorylated c-JUN, and AGR2 expression following c-JUN knockdown and IGF1 stimulation over time (performed in triplicate).

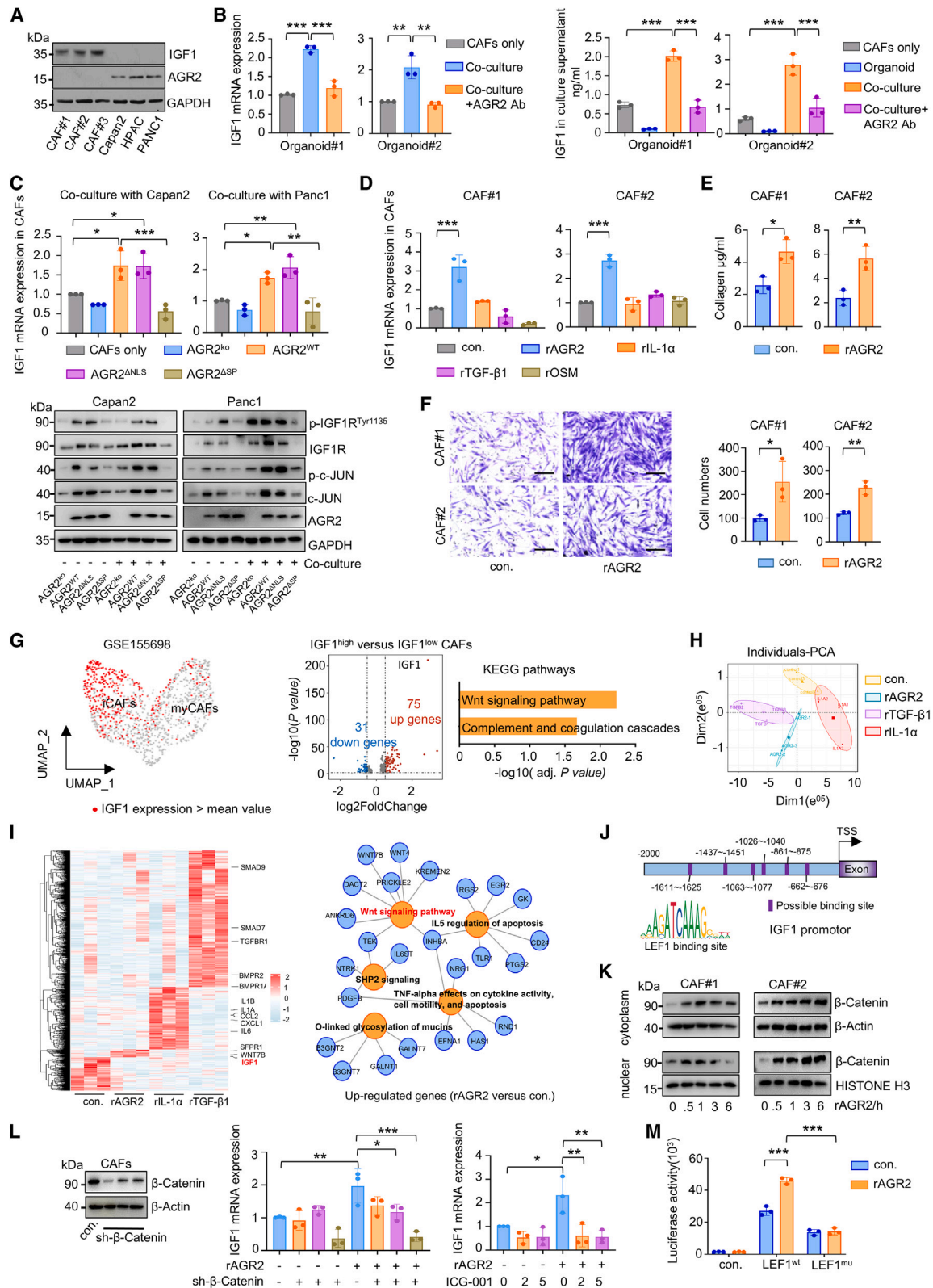
(L) Western blot shows c-JUN, phosphorylated c-JUN, and AGR2 expression post anisomycin treatment over time (performed in triplicate).

(M) Chromatin immunoprecipitation followed by quantitative PCR (ChIP-qPCR) demonstrates c-JUN enrichment at AGR2's transcription start sites (TSSs) before and after IGF1 treatment (performed in triplicate).

(N) Integrative Genomics Viewer (IGV) tracks display c-JUN peaks in AGR2's promoter region post IGF1 treatment.

(O) Dual-luciferase reporter assays in Capan2 and Panc1 cells evaluate AGR2 promoter activity under various lengths and site-specific mutations after IGF1 treatment (performed in triplicate).

Statistical analyses: (B) and (C) used a one-way ANOVA with multiple comparisons. (I), (M), (N), and (O) were analyzed using two-tailed, unpaired Student's t tests. Data are presented as mean  $\pm$  SD, with significance marked as \* $p < 0.05$ , \*\* $p < 0.01$ , \*\*\* $p < 0.001$ , and "ns" indicates no significance.



(legend on next page)

However, this effect was reduced in co-cultures without AGR2 secretion (AGR2<sup>KO</sup> or AGR2<sup>ΔSP</sup>). Notably, no significant change was observed in the expression of myCAF markers under these conditions (Figure S4B).

Among several cytokines tested (recombinant IL-1 $\alpha$  [rIL-1 $\alpha$ ], recombinant TGF- $\beta$ 1 [rTGF- $\beta$ 1], and recombinant oncostatin M), only recombinant AGR2 (rAGR2) significantly upregulated IGF1 expression in CAFs (Figure 4D). In parallel, rAGR2 also increased iCAF marker expression in CAFs, albeit with less potency than the classic iCAF inducer IL-1 $\alpha$  (Figure S4C). Additionally, rAGR2 treatment promoted CAF migration and collagen synthesis without affecting proliferation, demonstrating a multifaceted role of AGR2 in modulating CAF functions (Figures 4E and 4F; Figure S4D).

To identify the specific subtype of CAFs responsible for IGF1 production, we analyzed scRNA-seq data from 16 PDAC samples described by Steele et al. (GEO: GSE155698).<sup>25</sup> We found that iCAFs exhibited significantly higher levels of IGF1 expression compared to myCAFs (Figure 4G). When categorizing CAFs based on mean IGF expression into “high” or “low” expression groups, 41.73% of iCAFs were high expressers, compared to only 13.3% of myCAFs (Figures S4E and S4F). Further analysis of IGF1<sup>high</sup> versus IGF1<sup>low</sup> CAFs identified 106 DEGs (false discovery rate [FDR] < 0.01; fold change > log<sub>2</sub>(0.5)), 75 upregulated in IGF1<sup>high</sup> CAFs, forming an “IGF1-CAF signature.” Kyoto Encyclopedia of Genes and Genomes (KEGG) pathway analysis of these DEGs highlighted enrichment in “Wnt signaling” and “complement and coagulation cascades” (Figure 4G). Similar results were obtained from scRNA-seq data of 22 PDAC samples in Peng’s study (Genome Sequence Archive: PRJCA001063, Figures S4G–S4I).<sup>31</sup>

To explore the effects of rAGR2 on the CAF transcriptome, we performed RNA-seq after rAGR2 treatment, using TGF- $\beta$ 1 and

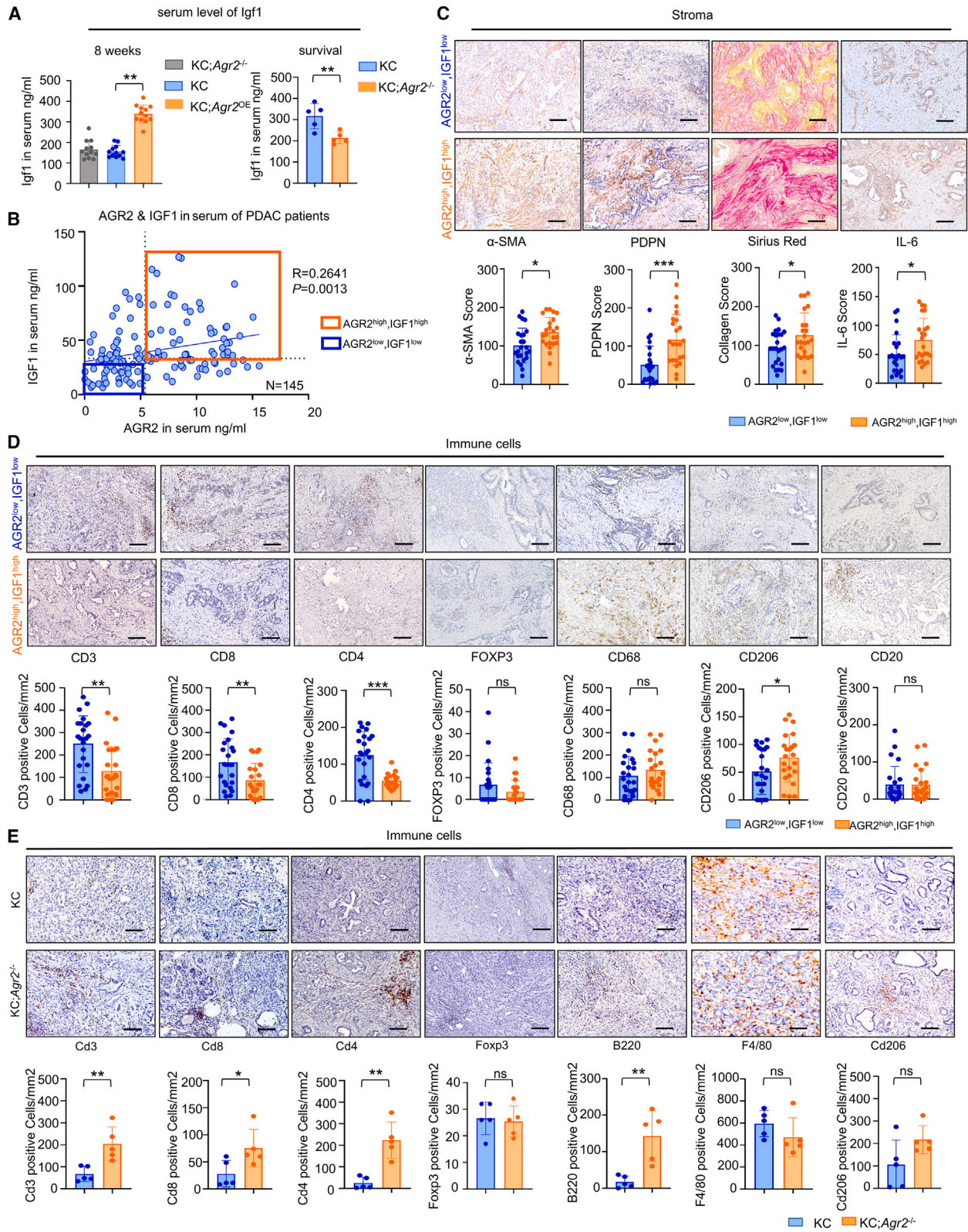
IL-1 $\alpha$  as controls. Principal component analysis demonstrated that rAGR2-treated samples formed a distinct cluster separate from rTGF- $\beta$ 1- or rIL-1 $\alpha$ -treated samples (Figure 4H). Among the altered genes, 224, including IGF1, were significantly upregulated post rAGR2 treatment. Functional annotation of these genes highlighted “Wnt signaling” as a key pathway (Figure 4I). Supporting the role of Wnt signaling in rAGR2-induced IGF1 expression, analysis of the *IGF1* promoter region uncovered several potential binding sequences for lymphoid enhancer binding factor 1 (LEF1), a key nuclear factor in the Wnt/ $\beta$ -catenin pathway (Figure 4J). This suggests potential transcriptional activation by Wnt signaling components, aligning with our findings of Wnt pathway enrichment in IGF1<sup>high</sup> CAFs and rAGR2-treated CAFs.

Given the established mechanism where AGR2 internalizes into NIH 3T3 cells through endocytosis, stabilizing  $\beta$ -catenin via direct binding and enhancing its nuclear accumulation,<sup>23</sup> we investigated whether a similar process occurs in primary PDAC-derived CAFs. Our findings reveal that CAFs internalize rAGR2 in a dose-dependent manner, a process inhibited by the endocytosis inhibitor Pistop2 (Figure S4J). Following rAGR2 treatment, we observed increased  $\beta$ -catenin levels in both the cytoplasm and nucleus of CAFs (Figure 4K). Further experiments demonstrated that  $\beta$ -catenin knockdown and the Wnt/ $\beta$ -catenin pathway inhibitor ICG-001 impaired rAGR2’s ability to promote IGF1 expression in CAFs (Figure 4L). This underscores the critical role of the Wnt/ $\beta$ -catenin signaling pathway in mediating the effects of rAGR2 on IGF1 production.

Next, we engineered several IGF1 promoter mutants and assessed their activity using luciferase reporter assays in CAFs. Mutations within the LEF1/T cell factor (TCF) consensus sequence significantly reduced IGF1 promoter activity,

#### Figure 4. Secreted AGR2 promotes IGF1 production from CAFs via the Wnt/ $\beta$ -catenin pathway

- (A) Western blot analysis evaluates AGR2 and IGF1 levels in three human PDAC-derived CAFs and three PDAC cell lines (Capan2, HPAC, and Panc1) across three independent experiments.
- (B) qRT-PCR analysis of IGF1 expression and supernatant ELISA analyses of IGF1 secretion in human PDAC-derived CAFs co-cultured with two human PDAC organoids and with or without treatment with Agr2-neutralizing antibody (5  $\mu$ g/mL) for 48 h ( $n = 3$  independent experiments).
- (C) qRT-PCR assesses IGF1 expression in PDAC-derived CAFs co-cultured with AGR2-knockout Capan2 and Panc1 cells, following re-expression of AGR2<sup>WT</sup>, AGR2<sup>ΔNLS</sup>, and AGR2<sup>ΔSP</sup> for 48 h (upper); Western blot analysis investigates IGF1R, phosphorylated IGF1R, c-JUN, phosphorylated c-JUN, and AGR2 levels in AGR2-knockout Capan2 and Panc1 cells after co-culture with PDAC-derived CAFs (lower,  $n = 3$  independent experiments).
- (D) qRT-PCR explores IGF1 expression in two PDAC-derived CAFs after treatment with rAGR2 (500 ng/mL), rTGF- $\beta$ 1 (4  $\mu$ g/mL), and rIL-1 $\alpha$  (200 ng/mL) for 24 h ( $n = 3$  independent experiments).
- (E) Supernatant analysis quantifies collagen levels in two PDAC-derived CAFs following rAGR2 treatment (500 ng/mL) for 24 h ( $n = 3$  independent experiments).
- (F) Transwell assays examine cell migration in two PDAC-derived CAFs following rAGR2 treatment (500 ng/mL) for 24 h ( $n = 3$  independent experiments).
- (G) Left: scRNA-seq identifies iCAFs and myCAFs within 16 PDAC tissues (GEO: GSE155698), showing iCAFs with elevated IGF1 expression (>mean value). Right: volcano plot displays genes differentially expressed between IGF1<sup>high</sup> and IGF1<sup>low</sup> CAFs (FDR < 0.01; log<sub>2</sub>FC > 0.5), accompanied by KEGG pathway analysis of the IGF1-CAF signature.
- (H) Principal component analysis (PCA) of transcriptomic data from CAFs treated with rAGR2, rTGF- $\beta$ 1, and rIL-1 $\alpha$  ( $n = 3$  per group).
- (I) A heatmap shows genes significantly upregulated in CAFs after treatment with rAGR2, rTGF- $\beta$ 1, and rIL-1 $\alpha$  (FDR < 0.01; log<sub>2</sub>FC > 0.5; left). Bioplant pathway analysis elucidates upregulated gene pathways post rAGR2 treatment in CAFs (right).
- (J) Identification of potential lymphoid enhancer binding factor 1 (LEF1)-binding sites within the IGF1 promoter region.
- (K) Western blot analysis shows  $\beta$ -catenin expression in both nuclear and cytoplasmic fractions of PDAC-derived CAFs after AGR2 stimulation (500 ng/mL) for 0.5, 1, 3, and 6 h ( $n = 3$  independent experiments).
- (L) Western blot and qRT-PCR analyses evaluate  $\beta$ -catenin and IGF1 levels in PDAC-derived CAFs post  $\beta$ -catenin knockdown or following treatment with ICG-001 (Wnt pathway inhibitor) and rAGR2 (500 ng/mL) for 24 h.
- (M) Luciferase reporter assays in three PDAC-derived CAFs transfected with wild-type and site-specific mutagenized IGF1 promoter sequences based on (J) predictions, post rAGR2 treatment (500 ng/mL) for 24 h ( $n = 3$  independent experiments).
- Statistical analysis: one-way ANOVA with multiple comparisons test was used for (B), (C), (D), and (L); two-tailed, unpaired Student’s *t* tests were employed for (E), (F), and (M). Data are presented as mean  $\pm$  SD, with \* $p < 0.05$ , \*\* $p < 0.01$ , \*\*\* $p < 0.001$  indicating levels of statistical significance.



(legend on next page)

underscoring the importance of this sequence in promoter functionality (Figure 4M). Despite these insights, we were unable to establish a direct interaction between  $\beta$ -catenin and rAGR2 in CAFs using a coIP assay.

In summary, PDAC-derived AGR2 influences multiple functions of CAFs in a paracrine manner, notably IGF1 production, by activating the Wnt/ $\beta$ -catenin signaling pathway.

### High serum levels of AGR2 and IGF1 are associated with enhanced desmoplastic reactions and immunosuppression in PDAC

We hypothesized that AGR2/IGF1-mediated paracrine and reciprocal signaling exacerbates desmoplastic reactions and tumorigenesis in PDAC. Supporting this hypothesis, we found that 8-week-old KC; *Agr2*<sup>OE</sup> mice had significantly elevated serum Igf1 levels compared to KC mice (Figure 5A). Additionally, phosphorylation levels of Igf1r and c-Jun were significantly higher in the pancreata of KC; *Agr2*<sup>OE</sup> mice (Figures S5A and S5B). In contrast, KC; *Agr2*<sup>-/-</sup> mice, which eventually developed PDAC, had significantly lower serum Igf1 levels and phosphorylated levels of Igf1r and c-Jun compared to KC mice with PDAC (Figure S5C).

To investigate clinical implications, we measured serum IGF1 levels in 145 patients with PDAC and noted a correlation with AGR2 levels (Figure 5B). Using the median value as a threshold, we categorized patients into four groups: AGR2<sup>high</sup>; IGF1<sup>high</sup> ( $n = 45$ ), AGR2<sup>high</sup>; IGF1<sup>low</sup> ( $n = 27$ ), AGR2<sup>low</sup>; IGF1<sup>high</sup> ( $n = 28$ ), and AGR2<sup>low</sup>; IGF1<sup>low</sup> ( $n = 45$ ). We then examined the association with tumor stroma by staining for CAF markers ( $\alpha$ -SMA, podoplanin [PDPN], and collagen, the latter detected with Sirius red and IL-6) and immune cell markers (CD3, CD4, CD8, FOXP3, CD68, CD206, and CD20). The staining intensity of  $\alpha$ -SMA, PDPN, collagen, and IL-6 staining was significantly more pronounced in AGR2<sup>high</sup>; IGF1<sup>high</sup> tumors compared to AGR2<sup>low</sup>; IGF1<sup>low</sup> tumors (Figure 5C). Additionally, AGR2<sup>high</sup>; IGF1<sup>high</sup> tumors exhibited a reduced infiltration of T cells (CD3<sup>+</sup>, CD4<sup>+</sup>, and CD8<sup>+</sup>) and an increased presence of M2 macrophages (CD206<sup>+</sup>) compared to AGR2<sup>low</sup>; IGF1<sup>low</sup> tumors (Figure 5D). Importantly, there was no statistically significant difference in the total counts of macrophages (CD68<sup>+</sup>), B cells (CD20<sup>+</sup>), and Tregs (FOXP3<sup>+</sup>) between the two groups (Figure 5D). This trend was similar in murine PDAC tumors derived from KC and KC; *Agr2*<sup>-/-</sup> mice, which showed an increased infiltration of T cells (Cd3<sup>+</sup>, Cd4<sup>+</sup>, and Cd8<sup>+</sup>) and B cells (B220<sup>+</sup>) in KC; *Agr2*<sup>-/-</sup> tumors (Figure 5E), without significant differences in total macrophage (F4/80<sup>+</sup>) or M2 macro-

phage (Cd206<sup>+</sup>) or Treg (Foxp3<sup>+</sup>) counts. Our findings suggest that AGR2/IGF1-mediated communication between cancer cells and CAFs exacerbates the desmoplastic response and may contribute to immunosuppression in PDAC.

### Combined targeting attenuates desmoplastic reaction and normalizes immunosuppressive microenvironment

To efficiently disrupt the crosstalk between PDAC cells and CAFs while circumventing compensatory pathways, we developed a therapeutic strategy combining an IGF1R inhibitor and an AGR2-neutralizing antibody. For preclinical testing, we first studied murine pancreatic stellate cells (PSCs), which are proposed as a source of CAFs in the PDAC stroma.<sup>32</sup> We found that cancer-naïve PSCs expressed higher levels of Igf1, similar to human CAFs, and that murine PDAC cells secreted substantial quantities of *Agr2* (Figure 6A).

We tested the effectiveness of this combined therapy in a co-culture system consisting of KPC organoids (derived from *Ptf1a*<sup>CreERTM</sup>; *LSL-Kras*<sup>G12D/+</sup>; *p53*<sup>fllox/fllox</sup> mice, hereafter “KPC”) and murine PSCs (Figure 6B). In co-culture, PSCs acquired a CAF phenotype and enhanced Igf1 secretion, as shown by increased mRNA levels and Igf1 protein concentration in the culture supernatant (Figure 6C). Treatment with either the IGF1R inhibitor (PPP), the *Agr2*-neutralizing antibody, or their combination reduced Igf1 production from CAFs. However, only the combined therapy significantly attenuated oncogenic mitogen-activated protein/extracellular signal-regulated kinase (Mek/Erk) signaling and reduced *Agr2* expression in KPC organoids (Figure 6D).

We evaluated the impact of treatment on CAF subtypes by analyzing the expression of specific subtype markers. The combined therapy notably decreased expression levels of iCAF markers, including *Il-1 $\alpha$* , *Il-6*, and *Lif*, while the expression of myCAF markers remained unchanged (Figure S6A). Notably, this dual inhibition strategy effectively suppressed the growth of KPC organoids in 3D culture (Figure 6E).

To evaluate the therapeutic efficacy *in vivo*, we treated a cohort of KPC mice with control antibodies ( $n = 5$ ), *Agr2*-neutralizing antibodies alone ( $n = 3$ ), IGF1R inhibitor alone ( $n = 3$ ), and a combination of *Agr2*-neutralizing antibodies and IGF1R inhibitor ( $n = 5$ ) for 2 weeks (Figure 6F). Remarkably, the combined therapy significantly reduced tumor volume, whereas the individual treatment exhibited only a modest effect.

ELISA assays revealed that *Agr2*-neutralizing antibodies reduced serum levels of *Agr2* in KPC mice. However, only the

### Figure 5. High serum levels of AGR2 and IGF1 are associated with enhanced desmoplastic reactions and immunosuppression in PDAC

(A) ELISA analysis of Igf1 in serum from 8-week-old KC mice, KC; *Agr2*<sup>-/-</sup> mice, and KC; *Agr2*<sup>OE</sup> mice reveals a significant difference (left,  $n = 12$  mice per group). Comparison between KC mice and KC; *Agr2*<sup>-/-</sup> mice with PDAC also shows marked differences (right,  $n = 5$  mice per group).

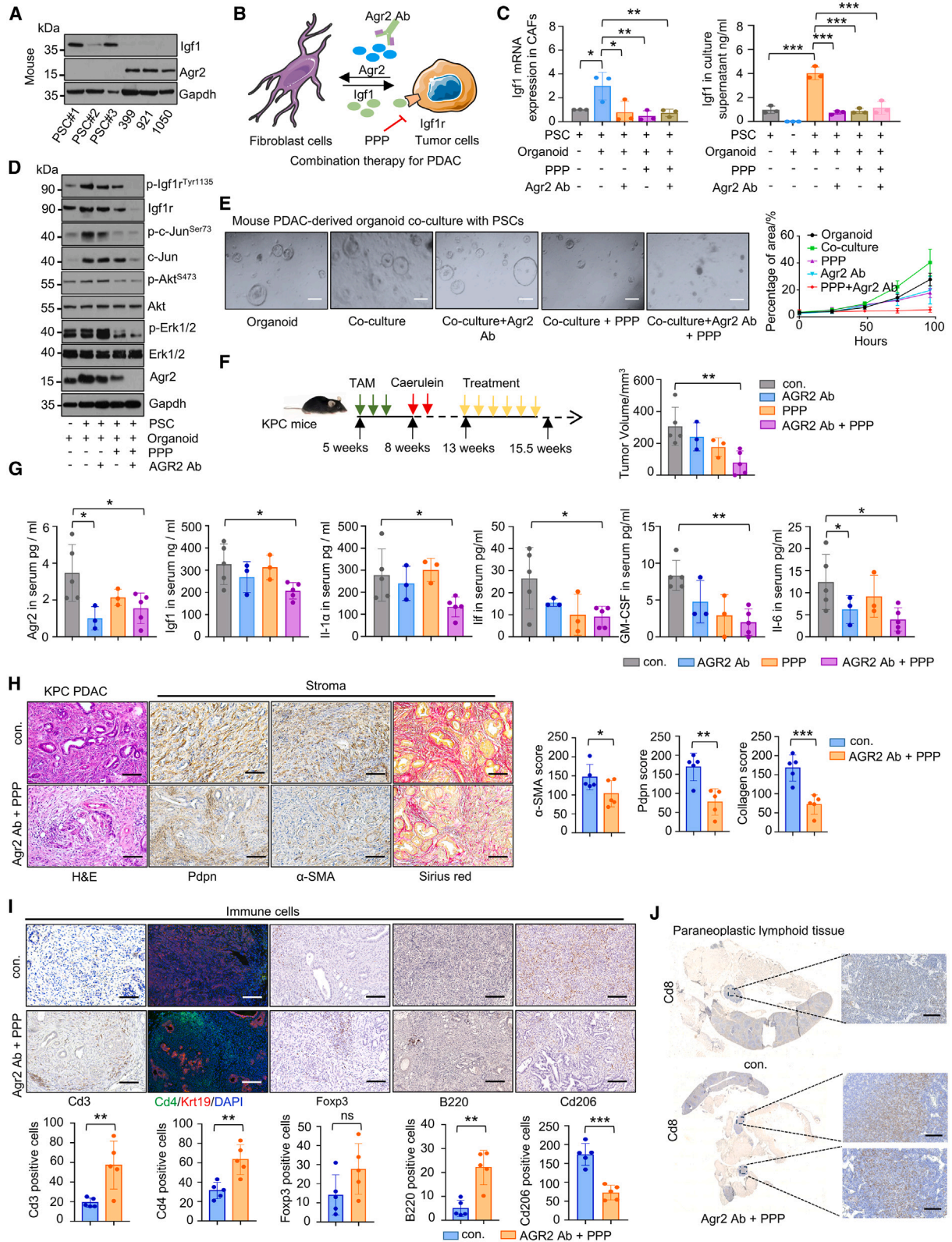
(B) Serum levels of AGR2 and IGF1 exhibit a correlation in 145 human patients with PDAC, analyzed using Pearson's correlation coefficient.

(C) IHC images display  $\alpha$ -SMA, podoplanin (PDPN), collagen, and IL-6 positivity in tumor areas, comparing AGR2<sup>high</sup>; IGF1<sup>high</sup> samples with AGR2<sup>low</sup>; IGF1<sup>low</sup> samples, demonstrating a difference in desmoplastic reaction.

(D) IHC images illustrate the differential presence of CD3, CD8, CD4, FOXP3, CD68, CD206, and CD20-positive cells in tumors between AGR2<sup>high</sup>; IGF1<sup>high</sup> samples and AGR2<sup>low</sup>; IGF1<sup>low</sup> samples, indicating variations in immune cell infiltration (scale bars: 50  $\mu$ m).

(E) IHC imaging further reveals the distribution of Cd3, Cd8, Cd4, Foxp3, B220, F4/80, and Cd206-positive cells in tumors from KC mice versus KC; *Agr2*<sup>-/-</sup> mice, emphasizing differences in immunological responses (scale bars: 50  $\mu$ m).

$p$  values in left of (A) was calculated using a one-way ANOVA with a multiple comparisons test,  $p$  values in right of (A), (C), (D), and (E) were calculated using two-tailed, unpaired Student's  $t$  tests, and correlation coefficient in (B) was calculated using Pearson's correlation coefficient. Data are presented as mean  $\pm$  SD. \* $p < 0.05$ , \*\* $p < 0.01$ , \*\*\* $p < 0.001$ . ns, no significance.



(legend on next page)

combined treatment of the Agr2-neutralizing antibody and IGF1R inhibitor significantly decreased serum levels of Igf1 and other iCAF-associated inflammatory cytokines including Il-1 $\alpha$ , Lif, granulocyte-macrophage colony-stimulating factor (GM-CSF), and Il-6 (Figure 6G). The combined therapy also reduced the desmoplastic reaction surrounding PDAC cells, as shown by hematoxylin and eosin,  $\alpha$ -SMA, Pdpn, and Sirius red staining (Figure 6H).

Additionally, this combined treatment attenuated the immunosuppressive milieu within PDAC tissues. Specifically, we observed a significant increase in the infiltration of T cells (CD3<sup>+</sup>), CD4<sup>+</sup> T cells, and B cells (B220<sup>+</sup>) post treatment, with no significant change in Treg (Foxp3<sup>+</sup>) infiltration (Figure 6I). Although CD8<sup>+</sup> T cells were not detected within PDAC tissues, they were notably enriched in the peripancreatic lymph nodes of treated mice, indicating enhanced anti-tumor immunity (Figure 6J). However, mature tertiary lymphoid structures were absent in both control and treated PDAC tissues. Meanwhile, combined therapy led to a marked decrease in the phosphorylation levels of Igf1r and p-c-Jun (Figures S6B and S6C), underscoring the disruption of key signaling pathways.

## DISCUSSION

Tumor cells in PDAC secrete proteins as paracrine signals to regulate the tumor microenvironment (TME), resulting in a highly desmoplastic and immunosuppressive state. Our study identified AGR2 as a crucial paracrine signaling factor that, along with CAF-derived reciprocal IGF1 signaling, forms a detrimental feedback loop, amplifying desmoplastic reactions, immunosuppression, and tumorigenesis in PDAC. Through *in vitro* and *in vivo* analyses, targeting the AGR2/IGF1 signaling loop using AGR2-neutralizing antibodies and IGF1R inhibitors showed promising anti-tumor effects by reducing desmoplasia and enhancing immunity.

Our preliminary findings reveal that AGR2 is a key protein involved in the tumorigenesis of PDAC.<sup>18</sup> AGR2 is ubiquitously expressed in PDAC tumor cells and precancerous lesions, conferring diverse functions. Recent research has unveiled

AGR2's role as a regulator of the inositol-requiring enzyme-1 $\beta$  (IRE1 $\beta$ ), crucial for maintaining ER homeostasis and the survival of mucin-producing intestinal goblet cells.<sup>33,34</sup> These insights are significant as the AGR2-IRE1 $\beta$  interaction is vital for the mucus production program, central to the classical PDAC phenotype characterized by gland-forming tumors within a dense, collagen-rich stroma.<sup>26,35</sup> Notably, AGR2 is a classical marker, and its secretion, coupled with its role in maintaining ER homeostasis, promotes CAF migration and collagen synthesis, aligning with the histological features of the classical subtype.<sup>36</sup>

Our study further identified AGR2 as a tumor cell-derived exocrine signal that plays a critical role in altering the immune cellular composition of the TME. This was confirmed by the strong correlation between AGR2 serum levels and immune composition in human PDAC samples and by gene editing to delete AGR2 in mice, replicating the phenotype.

Moreover, we have identified an IGF1-producing CAF subtype responsive to PDAC-derived AGR2, distinct from previously described CAF populations. Characterized by Wnt/ $\beta$ -catenin pathway activation, this IGF1-positive CAF subtype appears to play an immunosuppressive role in PDAC, which is partially overlapping with previously defined LRRC15-positive myCAFs.<sup>14,15</sup> Here, it underscores the need for further high-quality studies to elucidate the differential impacts of these CAF subtypes on the immune landscape and progression of PDAC. CAFs are pivotal in reshaping the immune microenvironment of PDAC and promoting tumorigenesis and malignant progression. Targeting CAFs has been a long-desired therapeutic approach against PDAC. It is increasingly recognized that CAFs are a heterogeneous subgroup, with evidence supporting three functionally distinct subtypes based on single-cell sequencing data: myCAFs, iCAFs, and apCAFs.<sup>9,10</sup> These subpopulations are dynamic and can transform under stimuli such as IL-1 and TGF- $\beta$ .<sup>37</sup> The signaling crosstalk between PDAC tumor cells and CAFs exacerbates this process. Some CAF subtypes contribute to the immunosuppressive state in PDAC. Our study identified an IGF1-producing CAF subtype responsive to PDAC-derived AGR2, characterized by Wnt/ $\beta$ -catenin

### Figure 6. Combined targeting attenuates desmoplastic reaction and normalizes immunosuppressive microenvironment

(A) Western blot analysis reveals Agr2 and Igf1 levels in PSCs isolated from wild-type mice and three mouse PDAC cell lines, highlighting the differential expression patterns.

(B) Schematic diagram shows the therapeutic strategy of combining IGF1R inhibitor and AGR2-neutralizing antibody.

(C) ELISA and qRT-PCR analyses demonstrate Igf1 levels in PSCs co-cultured with KPC PDAC-derived organoids. The impact of treatments with the IGF1R inhibitor (PPP; 1  $\mu$ M), Agr2-neutralizing antibody (5  $\mu$ g/mL) alone, or their combination for 48 h is shown ( $n = 3$  independent experiments).

(D) Western blot results display the expression levels of p-Igf1r, Igf1r, c-Jun, p-c-Jun, Akt, p-Akt, Erk, p-Erk, and Agr2 in mouse PDAC-derived organoids after co-culture with PSC cells and subsequent treatments as mentioned in (C) ( $n = 3$  independent experiments).

(E) Representative images and quantitative analyses show the growth dynamics of PDAC organoids co-cultured with PSC cells under various treatment conditions over 0, 24, 48, and 96 h (scale bars: 50  $\mu$ m,  $n = 3$  independent experiments).

(F) Tumor volume comparisons in KPC mice post caerulein-induced acute pancreatitis and subsequent treatments with Agr2 antibody (4 mg/kg; intraperitoneally [i.p.], three times per week for 2 weeks), PPP (20 mg/kg; i.p., three times per week for 2 weeks), or their combination ( $n = 5$  for control group,  $n = 3$  for single treatment groups, and  $n = 5$  for combined treatment group).

(G) ELISA quantification of Agr2, Igf1, Il-1 $\alpha$ , Lif, GM-CSF, and Il-6 in serum samples from the four groups of KPC mice underscores the systemic effects of the treatment modalities on cytokine levels ( $n = 5$  for control group,  $n = 3$  for single treatment groups, and  $n = 5$  for combined treatment group).

(H and I) Representative stained sections and quantitative statistics of H&E, Pdpn,  $\alpha$ -SMA, collagen, Cd3, Cd4, Foxp3, B220, and Cd206-positive cells within PDAC tumors (scale bars: 50  $\mu$ m,  $n = 5$  mice per group).

(J) Representative IHC highlights CD8-positive cells in lymph nodes adjacent to the tumors (scale bars: 50  $\mu$ m).

$p$  values in (C), (F), and (G) were calculated using a one-way ANOVA with a multiple comparisons test, and  $p$  values in (H) and (I) were calculated using two-tailed, unpaired Student's  $t$  tests. Data are presented as mean  $\pm$  SD. \* $p < 0.05$ , \*\* $p < 0.01$ , \*\*\* $p < 0.001$ .

pathway activation and playing an immunosuppressive role, partially overlapping with previously defined LRRC15-positive myCAFs.<sup>14,15</sup> This underscores the need for further studies to elucidate the differential impacts of these CAF subtypes on the immune landscape and PDAC progression.

Interestingly, our *in vitro* assays collectively demonstrate that secreted AGR2 primarily affects iCAF function rather than myCAF activity. However, when *Agr2* is genetically ablated in KC mice or neutralized in combination with IGF1R inhibition in *KPC* mice, we observe a reduction in the overall desmoplastic reaction in PDACs rather than a specific reduction in the iCAF population. These findings align with our observations in human samples. We propose that AGR2/IGF1-mediated crosstalk between PDAC cells and IGF1-positive CAFs plays a role in initiating and sustaining the desmoplastic response. Disruption of this crosstalk likely induces secondary effects on the local immune microenvironment, contributing to the observed reduction in the desmoplastic reaction. Similarly, while rAGR2 does not impact CAF proliferation *in vitro*, we observed increased CAF proliferation in KC; *Agr2*<sup>OE</sup> pancreata compared to KC pancreata *in vivo*. In addition to increased CAF proliferation, KC; *Agr2*<sup>OE</sup> pancreata exhibited significant alterations in tissue structures, including organ degeneration with proliferative ADM and PanIN lesions as well as increased immune cell infiltration. These findings suggest that the increased CAF proliferation in KC; *Agr2*<sup>OE</sup> pancreata likely reflects the outcome of complex intercellular interactions triggered by *Agr2*<sup>OE</sup> in epithelial cells. These seemingly discrepant *in vitro* and *in vivo* data underscore the important role of AGR2/IGF1-mediated crosstalk in supporting tissue homeostasis and modulating immune responses.

Fibroblasts were identified as the main source of IGF1 in the PDAC TME, with Shh secretion stimulating CAFs to produce IGF1 in the context of KRAS mutation.<sup>3</sup> Our data provide insights into IGF1 signaling regulation in PDAC. AGR2 not only accelerates IGF1 synthesis by CAFs but also stabilizes IGF1R, amplifying the signal. Thus, intervening in AGR2 can significantly antagonize IGF1 signaling. We generated a monoclonal neutralizing antibody targeting AGR2 and validated its therapeutic efficacy in combination with IGF1R inhibitors in co-culture systems of organoids and CAFs, as well as in a spontaneous PDAC animal model. This approach significantly attenuated IGF1 signaling in the TME, alleviating tumor progression. Pathological staining revealed a significant increase in immunoreactive cell subpopulations, including T cells and B cells, following treatment. These results suggest a promising alternative approach for targeted PDAC therapy.

Overall, we demonstrate the crucial role of tumor cell-secreted AGR2 in the IGF1 signaling pathway of PDAC, discovering a strategy for targeted therapy through the combination of AGR2-neutralizing antibodies and IGF1R inhibitors.

### Limitations of the study

This study primarily focuses on AGR2/IGF1-mediated cancer-CAF interactions within primary PDACs rather than metastatic sites. Recent findings by Khaliq et al. highlight the substantial heterogeneity of the TME between primary and metastatic sites, particularly in cancer-CAF interactions, suggesting a complexity greater than previously recognized.<sup>38</sup> Hence, it remains uncer-

tain whether disrupting AGR2/IGF1 paracrine and reciprocal signaling would be equally effective in metastatic PDACs. Additionally, the exact mechanisms by which AGR2/IGF1-mediated cancer-CAF interactions modulate the local immune TME are not yet fully understood, and we observed species-dependent differences. For example, more immunosuppressive M2 macrophages were present in human AGR2<sup>high</sup>; IGF1<sup>high</sup> PDACs, whereas this trend was not detected in murine PDACs. Further mechanistic studies in both human and murine PDAC models are needed to clarify these observations.

### RESOURCE AVAILABILITY

#### Lead contact

Further information and requests should be directed to and will be fulfilled by the lead contact, Bo Kong ([bo.kong@med.uni-heidelberg.de](mailto:bo.kong@med.uni-heidelberg.de)).

#### Materials availability

The *LSL-Rosa*<sup>CAG-Agr2</sup> line generated in this study will be made available as sperm upon request to the lead contact, but we may require a payment for transportation and a completed Materials Transfer Agreement if there is potential for commercial application. Additionally, all reagents generated in this study are available from the lead contact, subject to a completed Materials Transfer Agreement.

#### Date and code availability

- All sequencing data generated in this study have been deposited at the Gene Expression Omnibus under accession codes GEO: GSE264148 and GEO: GSE267820. This paper also analyses existing, publicly available single-cell sequencing data of human PDAC, sourced from GEO: GSE155698 in the Gene Expression Omnibus and PRJCA001063 in the Genome Sequence Archive.
- This paper does not report original code.
- Any additional information required to reanalyze the data reported in this paper is available from the lead contact upon reasonable request.

### ACKNOWLEDGMENTS

This project was supported in part by the AiF Projekt (ZIM-Kooperationsprojekte, Central Innovation Program Cooperation Projects, ZF4353701SK6 and KK5170601AD0 to B.K.), German Cancer Aid Foundation (Deutsche Krebshilfe, 70113828, to B.K.), German Research Foundation (DFG, KO 4369/4-1 and KO 4369/6-1 to B.K.), Hans Beger Stiftung (Nr.17-02-2022, to B.K.), Wilhelm Sander-Stiftung (Nr. 2022.135.1, to B.K.), National Natural Science Foundation of China (82072651, 82072652, 81871947, 81602147, 82203657, and 82203330), Natural Science Foundation of Jiangsu Province (BK20220190), China Postdoctoral Science Foundation (2022M711584 and 2022M711589), Sino-German Mobility Programme (M-0251), Jiangsu Provincial Health Commission Science Foundation (M2021002), Jiangsu province major disease biobank opening project - pancreas disease biobank (SBK202001001), Nanjing health science and technology development general project (YKK20055), and Nanjing Drum Tower Hospital clinical research and cultivation project (2021-LCYJ-PY-26). S.N., H.L., and S.Z. received a fellowship from the Scholarship Council of the Ministry of Education of China.

### AUTHOR CONTRIBUTIONS

B.K. designed the study. B.K. and S.S. coordinated and co-supervised the study. H.L., Z.Z., Z.S., S.Z., S.N., Y.Y., L.Z., Y. Sun, C.F., J.H., Y.N., K.S., L.W., K.J., and Z.L. performed the experiments and acquired data. C.K., S.R., M.L., I.H., Y. Sunami, J.K., H.F., M.R., Z.D., X.Z., and C.W.M. critically revised the manuscript and contributed intellectual content. B.K., H.L., and I.H. drafted the manuscript. All authors approved the final version of the manuscript.

### DECLARATION OF INTERESTS

The authors declare no competing interests.

### STAR★METHODS

Detailed methods are provided in the online version of this paper and include the following:

- **KEY RESOURCES TABLE**
- **EXPERIMENTAL MODEL AND STUDY PARTICIPANT DETAILS**
  - Patient material and tissues
  - Transgenic mice
  - *In vivo* transplantation assays
  - Treatment of KPC mice
  - Cell lines and culture
- **METHOD DETAILS**
  - AAV vector production and transduction
  - Human and mouse PDAC-derived organoid isolation and passage
  - Isolation of human CAFs
  - Isolation of mouse PSCs
  - Co-culture of tumor organoids and CAFs/PSCs
  - AGR2 knockout cell lines
  - shRNA and siRNA knockdown studies
  - Plasmid generation
  - ELISA assay
  - Western blot
  - Flow cytometry analysis
  - Luciferase reporter assay
  - Immunohistochemistry and immunofluorescence staining of tissue
  - If staining of cells
  - qRT-PCR
  - Protein extraction from subcellular fractions
  - Chromatin immunoprecipitation (CHIP) qPCR
  - Co-immunoprecipitation
  - Transwell assay
  - RNA sequencing
  - Cut&Tag sequencing
  - Detection of collagen in culture medium
  - Construction of AGR2 neutralizing antibody
  - Single cell data analysis
- **QUANTIFICATION AND STATISTICAL ANALYSIS**

### SUPPLEMENTAL INFORMATION

Supplemental information can be found online at <https://doi.org/10.1016/j.xcrm.2024.101927>.

Received: June 19, 2024

Revised: November 6, 2024

Accepted: December 30, 2024

Published: February 6, 2025

### REFERENCES

1. Kong, B., Bruns, P., Behler, N.A., Chang, L., Schlitter, A.M., Cao, J., Gewies, A., Ruland, J., Fritzsche, S., Valkovskaya, N., et al. (2018). Dynamic landscape of pancreatic carcinogenesis reveals early molecular networks of malignancy. *Gut* 67, 146–156. <https://doi.org/10.1136/gutjnl-2015-310913>.
2. Li, J., and Stanger, B.Z. (2019). The tumor as organizer model. *Science* 363, 1038–1039. <https://doi.org/10.1126/science.aau9861>.
3. Tape, C.J., Ling, S., Dimitriadis, M., McMahon, K.M., Worboys, J.D., Leong, H.S., Norrie, I.C., Miller, C.J., Pouligiannis, G., Lauffenburger, D.A., and Jørgensen, C. (2016). Oncogenic KRAS Regulates Tumor Cell Signaling via Stromal Reciprocation. *Cell* 165, 910–920. <https://doi.org/10.1016/j.cell.2016.03.029>.
4. Olive, K.P., Jacobetz, M.A., Davidson, C.J., Gopinathan, A., McIntyre, D., Honess, D., Madhu, B., Goldgraben, M.A., Caldwell, M.E., Allard, D., et al. (2009). Inhibition of Hedgehog signaling enhances delivery of chemotherapy in a mouse model of pancreatic cancer. *Science* 324, 1457–1461. <https://doi.org/10.1126/science.1171362>.
5. Ireland, L., Santos, A., Ahmed, M.S., Rainer, C., Nielsen, S.R., Quaranta, V., Weyer-Czernilofsky, U., Engle, D.D., Perez-Mancera, P.A., Coupland, S.E., et al. (2016). Chemoresistance in Pancreatic Cancer Is Driven by Stroma-Derived Insulin-Like Growth Factors. *Cancer Res.* 76, 6851–6863. <https://doi.org/10.1158/0008-5472.CAN-16-1201>.
6. Ko, A.H., LoConte, N., Tempero, M.A., Walker, E.J., Kate Kelley, R., Lewis, S., Chang, W.C., Kantoff, E., Vannier, M.W., Catenacci, D.V., et al. (2016). A Phase I Study of FOLFIRINOX Plus IPI-926, a Hedgehog Pathway Inhibitor, for Advanced Pancreatic Adenocarcinoma. *Pancreas* 45, 370–375. <https://doi.org/10.1097/MPA.0000000000000458>.
7. Fuchs, C.S., Azevedo, S., Okusaka, T., Van Laethem, J.L., Lipton, L.R., Riess, H., Szczylk, C., Moore, M.J., Peeters, M., Bodoky, G., et al. (2015). A phase 3 randomized, double-blind, placebo-controlled trial of ganitumab or placebo in combination with gemcitabine as first-line therapy for metastatic adenocarcinoma of the pancreas: the GAMMA trial. *Ann. Oncol.* 26, 921–927. <https://doi.org/10.1093/annonc/mdv027>.
8. Ohlund, D., Handy-Santana, A., Biffi, G., Elyada, E., Almeida, A.S., Ponz-Sarvisé, M., Corbo, V., Oni, T.E., Hearn, S.A., Lee, E.J., et al. (2017). Distinct populations of inflammatory fibroblasts and myofibroblasts in pancreatic cancer. *J. Exp. Med.* 214, 579–596. <https://doi.org/10.1084/jem.20162024>.
9. Elyada, E., Bolisetty, M., Laise, P., Flynn, W.F., Courtois, E.T., Burkhart, R.A., Teinor, J.A., Belleau, P., Biffi, G., Lucito, M.S., et al. (2019). Cross-Species Single-Cell Analysis of Pancreatic Ductal Adenocarcinoma Reveals Antigen-Presenting Cancer-Associated Fibroblasts. *Cancer Discov.* 9, 1102–1123. <https://doi.org/10.1158/2159-8290.CD-19-0094>.
10. Biffi, G., Oni, T.E., Spielman, B., Hao, Y., Elyada, E., Park, Y., Preall, J., and Tuveson, D.A. (2019). IL1-Induced JAK/STAT Signaling Is Antagonized by TGFβ to Shape CAF Heterogeneity in Pancreatic Ductal Adenocarcinoma. *Cancer Discov.* 9, 282–301. <https://doi.org/10.1158/2159-8290.CD-18-0710>.
11. Huang, H., Wang, Z., Zhang, Y., Pradhan, R.N., Ganguly, D., Chandra, R., Murimwa, G., Wright, S., Gu, X., Maddipati, R., et al. (2022). Mesothelial cell-derived antigen-presenting cancer-associated fibroblasts induce expansion of regulatory T cells in pancreatic cancer. *Cancer Cell* 40, 656–673. <https://doi.org/10.1016/j.ccell.2022.04.011>.
12. Chen, Y., Kim, J., Yang, S., Wang, H., Wu, C.J., Sugimoto, H., LeBleu, V.S., and Kalluri, R. (2021). Type I collagen deletion in alphaSMA(+) myofibroblasts augments immune suppression and accelerates progression of pancreatic cancer. *Cancer Cell* 39, 548–565. <https://doi.org/10.1016/j.ccell.2021.02.007>.
13. Sun, X., He, X., Zhang, Y., Hosaka, K., Andersson, P., Wu, J., Wu, J., Jing, X., Du, Q., Hui, X., et al. (2022). Inflammatory cell-derived CXCL3 promotes pancreatic cancer metastasis through a novel myofibroblast-hijacked cancer escape mechanism. *Gut* 71, 129–147. <https://doi.org/10.1136/gutjnl-2020-322744>.
14. Dominguez, C.X., Müller, S., Keerthivasan, S., Koeppen, H., Hung, J., Gierke, S., Breart, B., Foreman, O., Bainbridge, T.W., Castiglioni, A., et al. (2020). Single-cell RNA sequencing reveals stromal evolution into LRRC15+ myofibroblasts as a determinant of patient response to cancer immunotherapy. *Cancer Discov.* 10, 232–253.
15. Krishnamurthy, A.T., Shyer, J.A., Thai, M., Gandham, V., Buechler, M.B., Yang, Y.A., Pradhan, R.N., Wang, A.W., Sanchez, P.L., Qu, Y., et al. (2022). LRRC15(+) myofibroblasts dictate the stromal setpoint to suppress tumour immunity. *Nature* 611, 148–154. <https://doi.org/10.1038/s41586-022-05272-1>.

16. Chevet, E., Fessart, D., Delom, F., Mulot, A., Vojtesek, B., Hrstka, R., Murray, E., Gray, T., and Hupp, T. (2013). Emerging roles for the pro-oncogenic anterior gradient-2 in cancer development. *Oncogene* 32, 2499–2509. <https://doi.org/10.1038/onc.2012.346>.
17. Moidu, N.A., A Rahman, N.S., Syafruddin, S.E., Low, T.Y., and Mohtar, M.A. (2020). Secretion of pro-oncogenic AGR2 protein in cancer. *Heliyon* 6, e05000. <https://doi.org/10.1016/j.heliyon.2020.e05000>.
18. Zhang, Z., Li, H., Deng, Y., Schuck, K., Raulefs, S., Maeritz, N., Yu, Y., Hechler, T., Pahl, A., Fernández-Sáiz, V., et al. (2021). AGR2-Dependent Nuclear Import of RNA Polymerase II Constitutes a Specific Target of Pancreatic Ductal Adenocarcinoma in the Context of Wild-Type p53. *Gastroenterology* 161, 1601–1614. <https://doi.org/10.1053/j.gastro.2021.07.030>.
19. Tsuji, T., Satoyoshi, R., Aiba, N., Kubo, T., Yanagihara, K., Maeda, D., Goto, A., Ishikawa, K., Yashiro, M., and Tanaka, M. (2015). Agr2 mediates paracrine effects on stromal fibroblasts that promote invasion by gastric signet-ring carcinoma cells. *Cancer Res.* 75, 356–366. <https://doi.org/10.1158/0008-5472.CAN-14-1693>.
20. Maurel, M., Obacz, J., Avril, T., Ding, Y.P., Papadodima, O., Treton, X., Daniel, F., Pilalis, E., Hörberg, J., Hou, W., et al. (2019). Control of anterior Gradient 2 (AGR2) dimerization links endoplasmic reticulum proteostasis to inflammation. *EMBO Mol. Med.* 11, e10120. <https://doi.org/10.15252/emmm.201810120>.
21. Tiemann, K., Garri, C., Lee, S.B., Malihi, P.D., Park, M., Alvarez, R.M., Yap, L.P., Mallick, P., Katz, J.E., Gross, M.E., and Kani, K. (2019). Loss of ER retention motif of AGR2 can impact mTORC signaling and promote cancer metastasis. *Oncogene* 38, 3003–3018. <https://doi.org/10.1038/s41388-018-0638-9>.
22. Tian, S., Hu, J., Tao, K., Wang, J., Chu, Y., Li, J., Liu, Z., Ding, X., Xu, L., Li, Q., et al. (2018). Secreted AGR2 promotes invasion of colorectal cancer cells via Wnt11-mediated non-canonical Wnt signaling. *Exp. Cell Res.* 364, 198–207. <https://doi.org/10.1016/j.yexcr.2018.02.004>.
23. Merugu, S.B., Zhou, B., Mangukiya, H.B., Negi, H., Ghulam, R., Roy, D., Qudsia, S., Wang, Z., Mashausi, D.S., Yunus, F.U.N., et al. (2021). Extracellular AGR2 activates neighboring fibroblasts through endocytosis and direct binding to beta-catenin that requires AGR2 dimerization and adhesion domains. *Biochem. Biophys. Res. Commun.* 573, 86–92. <https://doi.org/10.1016/j.bbrc.2021.08.028>.
24. Mangukiya, H.B., Negi, H., Merugu, S.B., Sehar, Q., Mashausi, D.S., Yunus, F.U.N., Wu, Z., and Li, D. (2019). Paracrine signalling of AGR2 stimulates RhoA function in fibroblasts and modulates cell elongation and migration. *Cell Adhes. Migrat.* 13, 332–344. <https://doi.org/10.1080/19336918.2019.1685928>.
25. Steele, N.G., Carpenter, E.S., Kemp, S.B., Sirihorachai, V.R., The, S., Delrosario, L., Lazarus, J., Amir, E.A.D., Gunchick, V., Espinoza, C., et al. (2020). Multimodal Mapping of the Tumor and Peripheral Blood Immune Landscape in Human Pancreatic Cancer. *Nat. Can. (Ott.)* 1, 1097–1112. <https://doi.org/10.1038/s43018-020-00121-4>.
26. Tonelli, C., Yordanov, G.N., Hao, Y., Deschênes, A., Hinds, J., Belleau, P., Klingbeil, O., Brosnan, E., Doshi, A., Park, Y., et al. (2024). A mucus production programme promotes classical pancreatic ductal adenocarcinoma. *Gut* 73, 941–954. <https://doi.org/10.1136/gutjnl-2023-329839>.
27. Dumartin, L., Alrawashdeh, W., Trabulo, S.M., Radon, T.P., Steiger, K., Feakins, R.M., di Magliano, M.P., Heesch, C., Esposito, I., Lemoine, N.R., and Crnogorac-Jurcevic, T. (2017). ER stress protein AGR2 precedes and is involved in the regulation of pancreatic cancer initiation. *Oncogene* 36, 3094–3103. <https://doi.org/10.1038/onc.2016.459>.
28. Dong, A., Wodziak, D., and Lowe, A.W. (2015). Epidermal growth factor receptor (EGFR) signaling requires a specific endoplasmic reticulum thioredoxin for the post-translational control of receptor presentation to the cell surface. *J. Biol. Chem.* 290, 8016–8027. <https://doi.org/10.1074/jbc.M114.623207>.
29. Hoyne, P.A., Elleman, T.C., Adams, T.E., Richards, K.M., and Ward, C.W. (2000). Properties of an insulin receptor with an IGF-1 receptor loop exchange in the cysteine-rich region. *FEBS Lett.* 469, 57–60. [https://doi.org/10.1016/S0014-5793\(00\)01237-0](https://doi.org/10.1016/S0014-5793(00)01237-0).
30. Zhu, Q., Mangukiya, H.B., Mashausi, D.S., Guo, H., Negi, H., Merugu, S.B., Wu, Z., and Li, D. (2017). Anterior gradient 2 is induced in cutaneous wound and promotes wound healing through its adhesion domain. *FEBS J.* 284, 2856–2869. <https://doi.org/10.1111/febs.14155>.
31. Peng, J., Sun, B.F., Chen, C.Y., Zhou, J.Y., Chen, Y.S., Chen, H., Liu, L., Huang, D., Jiang, J., Cui, G.S., et al. (2019). Single-cell RNA-seq highlights intra-tumoral heterogeneity and malignant progression in pancreatic ductal adenocarcinoma. *Cell Res.* 29, 725–738. <https://doi.org/10.1038/s41422-019-0195-y>.
32. Yu, Y., Schuck, K., Friess, H., and Kong, B. (2021). Targeting Aggressive Fibroblasts to Enhance the Treatment of Pancreatic Cancer. *Expert Opin. Ther. Targets* 25, 5–13. <https://doi.org/10.1080/14728222.2021.1857727>.
33. Cloots, E., Guilbert, P., Provost, M., Neidhardt, L., Van de Velde, E., Fayazpour, F., De Sutter, D., Savvides, S.N., Eyckerman, S., and Janssens, S. (2024). Activation of goblet-cell stress sensor IRE1beta is controlled by the mucin chaperone AGR2. *EMBO J.* 43, 695–718. <https://doi.org/10.1038/s44318-023-00015-y>.
34. Neidhardt, L., Cloots, E., Friemel, N., Weiss, C.A.M., Harding, H.P., McLaughlin, S.H., Janssens, S., and Ron, D. (2024). The IRE1beta-mediated unfolded protein response is repressed by the chaperone AGR2 in mucin producing cells. *EMBO J.* 43, 719–753. <https://doi.org/10.1038/s44318-023-00014-z>.
35. Kalimuthu, N.S., Wilson, G.W., Grant, R.C., Seto, M., O’Kane, G., Vajpeyi, R., Notta, F., Gallinger, S., and Chetty, R. (2020). Morphological classification of pancreatic ductal adenocarcinoma that predicts molecular subtypes and correlates with clinical outcome. *Gut* 69, 317–328. <https://doi.org/10.1136/gutjnl-2019-318217>.
36. Moffitt, R.A., Marayati, R., Flate, E.L., Volmar, K.E., Loeza, S.G.H., Hoadley, K.A., Rashid, N.U., Williams, L.A., Eaton, S.C., Chung, A.H., et al. (2015). Virtual microdissection identifies distinct tumor- and stroma-specific subtypes of pancreatic ductal adenocarcinoma. *Nat. Genet.* 47, 1168–1178. <https://doi.org/10.1038/ng.3398>.
37. Steele, N.G., Biffi, G., Kemp, S.B., Zhang, Y., Drouillard, D., Syu, L., Hao, Y., Oni, T.E., Brosnan, E., Elyada, E., et al. (2021). Inhibition of Hedgehog Signaling Alters Fibroblast Composition in Pancreatic Cancer. *Clin. Cancer Res.* 27, 2023–2037. <https://doi.org/10.1158/1078-0432.CCR-20-3715>.
38. Khaliq, A.M., Rajamohan, M., Saeed, O., Mansouri, K., Adil, A., Zhang, C., Turk, A., Carstens, J.L., House, M., Hayat, S., et al. (2024). Spatial transcriptomic analysis of primary and metastatic pancreatic cancers highlights tumor microenvironmental heterogeneity. *Nat. Genet.* 56, 2455–2465. <https://doi.org/10.1038/s41588-024-01914-4>.
39. Kong, B., Wu, W., Cheng, T., Schlitter, A.M., Qian, C., Bruns, P., Jian, Z., Jäger, C., Regel, I., Raulefs, S., et al. (2016). A subset of metastatic pancreatic ductal adenocarcinomas depends quantitatively on oncogenic Kras/Mek/Erk-induced hyperactive mTOR signalling. *Gut* 65, 647–657. <https://doi.org/10.1136/gutjnl-2014-307616>.
40. Bachem, M.G., Schünemann, M., Ramadani, M., Siech, M., Beger, H., Buck, A., Zhou, S., Schmid-Kotsas, A., and Adler, G. (2005). Pancreatic carcinoma cells induce fibrosis by stimulating proliferation and matrix synthesis of stellate cells. *Gastroenterology* 128, 907–921.
41. Apte, M.V., Haber, P.S., Applegate, T.L., Norton, I.D., McCaughan, G.W., Korsten, M.A., Pirola, R.C., and Wilson, J.S. (1998). Periacinar stellate shaped cells in rat pancreas: identification, isolation, and culture. *Gut* 43, 128–133. <https://doi.org/10.1136/gut.43.1.128>.

STAR★METHODS

KEY RESOURCES TABLE

REAGENT or RESOURCE	SOURCE	IDENTIFIER
<b>Antibodies</b>		
Rabbit monoclonal anti-AGR2	Abcam	Cat# Ab76473; RRID: AB_1565853
Mouse monoclonal anti-AGR2	Santa Cruz Biotechnology	Cat# sc-101211; RRID: AB_2225121
Rabbit polyclonal anti-AGR2	Invitrogen	Cat# PA5-85636; RRID: AB_2792776
Mouse monoclonal anti-PDPN	BioLegend	Cat# 395002; RRID: AB_2750203
Syrian Hamster monoclonal anti-PDPN	BioLegend	Cat# 127409; RRID: AB_10612940
Rabbit monoclonal anti-IGF-I Receptor $\beta$	Cell Signaling Technology	Cat# 9750; RRID: AB_10950969
Rabbit monoclonal anti-Phospho-IGF-I Receptor $\beta$	Cell Signaling Technology	Cat# 3918
Rabbit polyclonal anti-Ki-67	Abcam	Cat# Ab15580; RRID: AB_443209
Rabbit monoclonal anti-c-JUN	Cell Signaling Technology	Cat# 9165; RRID: AB_2130165
Rabbit monoclonal anti-Phospho-c-JUN	Cell Signaling Technology	Cat# 3270; RRID: AB_2129575
Rabbit monoclonal anti- $\alpha$ -SMA	Cell Signaling Technology	Cat# 19245; RRID: AB_2734735
Mouse monoclonal anti- $\alpha$ -SMA	Agilent	Cat# M0851; RRID: AB_2223500
Rabbit monoclonal anti-GAPDH	Cell Signaling Technology	Cat# 2118; RRID: AB_561053
Rabbit anti-Beta Actin	Proteintech	Cat# 81115-1-RR; RRID: AB_2923704
Rabbit polyclonal anti-Histone H3	Cell Signaling Technology	Cat# 9715; RRID: AB_331563
Rabbit monoclonal anti-Phospho-Histone H3	Cell Signaling Technology	Cat# 53348; RRID: AB_2799431
Rabbit monoclonal anti-BIP	Cell Signaling Technology	Cat# 3177; RRID: AB_2119845
Rabbit polyclonal anti-Na, K-ATPase	Cell Signaling Technology	Cat# 3010; RRID: AB_2060983
Rabbit polyclonal anti-AKT	Cell Signaling Technology	Cat# 9272; RRID: AB_329827
Rabbit monoclonal anti-Phospho-AKT	Cell Signaling Technology	Cat# 4060; RRID: AB_2315049
Rabbit monoclonal anti-PI3K	Cell Signaling Technology	Cat# 4249; RRID: AB_2165248
Mouse monoclonal anti-IGF1	Santa Cruz Biotechnology	Cat# sc-518040;
Mouse monoclonal anti-Krt19	DSHB	Cat# AB_2133570
Rabbit monoclonal anti- $\alpha$ -Amylase	Cell Signaling Technology	Cat# 3796; RRID: AB_2226822
Mouse monoclonal anti-BrdU	Cell Signaling Technology	Cat# 5292; RRID: AB_10548898
Mouse monoclonal anti-MUC5AC	Abcam	Cat# ab3649; RRID: AB_2146844
Rabbit monoclonal anti-Erk1/2	Cell Signaling Technology	Cat# 4695; RRID: AB_390779
Rabbit monoclonal anti-Phospho-Erk1/2	Cell Signaling Technology	Cat# 4370; RRID: AB_2315112
Mouse monoclonal anti- $\beta$ -Catenin	Proteintech	Cat# 66379-1-Ig; RRID: AB_2857358
Mouse monoclonal anti-CD3	Agilent	Cat# M7254; RRID: AB_2631163
Rabbit monoclonal anti-CD3	Abcam	Cat# ab16669; RRID: AB_443425
Rabbit monoclonal anti-CD4	Abcam	Cat# ab183685; RRID: AB_2686917
Mouse monoclonal anti-CD8	Agilent	Cat# M7103; RRID: AB_2075537
Rabbit monoclonal anti-CD8	Cell Signaling Technology	Cat# 98941; RRID: AB_2756376
Rabbit monoclonal anti-Foxp3	Cell Signaling Technology	Cat# 98377; RRID: AB_2747370
Rabbit monoclonal anti-Foxp3	Cell Signaling Technology	Cat# 12653; RRID: AB_2797979
Mouse monoclonal anti-IL-6	Abcam	Cat# ab9324; RRID: AB_307175
Rabbit monoclonal anti-Insulin	Cell Signaling Technology	Cat# 3014; RRID: AB_2126503
Mouse monoclonal anti-CD68	Abcam	Cat# ab955; RRID: AB_307338
Rabbit monoclonal anti-CD206	Cell Signaling Technology	Cat# 24595; RRID: AB_2892682
Rabbit monoclonal anti-CD20	Abcam	Cat# ab78237; RRID: AB_1640323
Rat monoclonal anti-B220	BioLegend	Cat# 103203; RRID: AB_312988

(Continued on next page)

**Continued**

REAGENT or RESOURCE	SOURCE	IDENTIFIER
Rabbit monoclonal anti-F4/80	Abcam	Cat# ab300421; RRID: AB_2936298
Monoclonal AGR2-neutralizing antibody	Abcam	N/A
Goat anti-rabbit IgG, HRP-linked	Cell Signaling Technology	Cat# 7074; RRID: AB_2099233
Horse anti-mouse IgG, HRP-linked	Cell Signaling Technology	Cat# 7076; RRID: AB_330924
Rabbit Anti-Syrian Hamster IgG H&L	Abcam	Cat# ab6699; RRID: AB_955992
Rabbit Anti-Rat IgG H&L (HRP)	Abcam	Cat# ab6734; RRID: AB_955450
Goat Anti-Rat IgG H&L (Alexa Fluor® 647)	Abcam	Cat# ab150159; RRID: AB_2566823
Goat Anti-Mouse IgG H&L (Alexa Fluor® 488)	Abcam	Cat# ab150113; RRID: AB_2576208
Goat Anti-Rabbit IgG H&L (Alexa Fluor® 594)	Abcam	Cat# ab150080; RRID: AB_2650602
<b>Bacterial and virus strains</b>		
AAV8-Agr2 <sup>WT</sup>	GENECHEM	N/A
AAV8-Agr2 <sup>ΔSP</sup>	GENECHEM	N/A
<b>Biological samples</b>		
Human PDAC tissue and serum samples	Klinikum rechts der Isar, the First Affiliated Hospital of Nanjing Medical University, and Nanjing Drum Tower Hospital	N/A
<b>Chemicals, peptides, and recombinant proteins</b>		
Anisomycin	Selleck	Cat# S7409; CAS: 22862-76-6
Picropodophyllin (PPP)	Selleck	Cat# S7668; CAS: 477-47-4
3-Methyladenine (3-MA)	Selleck	Cat# S2767; CAS: 5142-23-4
Bafilomycin	Selleck	Cat# S1413; CAS: 88899-55-2
Chloroquine (NSC-187208)	Selleck	Cat# S6999; CAS: 54-05-7
MG-132	Selleck	Cat# S2619; CAS: 1211877-36-9
Pevonedistat (MLN4924)	Selleck	Cat# S7109; CAS: 905579-51-3
Foscarnivint (ICG-001)	Selleck	Cat# S2662; CAS: 847591-62-2
Pitstop 2	MedChemExpress	Cat# HY-115604; CAS: 1419320-73-2
Wortmannin	MedChemExpress	Cat# HY-10197; CAS: 19545-26-7
Rec. human AGR2 His-tag	R&D Systems	Cat# 10326-AG; GenPept: O95994
Rec. human IGF-1	R&D Systems	Cat# 291-G1; GenPept: P05019
Rec. human IL-1 $\alpha$ Protein	R&D Systems	Cat# 200-LA; GenPept: P01583
Rec. human TGF- $\beta$ 1	R&D Systems	Cat# 240-B; GenPept: P01137
InVivoMAb human IgG1 isotype control	BioXcell	Cat# BE0297
<b>Critical commercial assays</b>		
Human IGF-1 Quantikine ELISA Kit	R&D Systems	Cat# DG100B
Human AGR2 Quantikine ELISA Kit	Novus Biologicals	Cat# NBP2-78743
Mouse/rat IGF-1 Quantikine ELISA Kit	R&D Systems	Cat# MG100
Mouse IL-1 $\alpha$ Quantikine ELISA Kit	R&D Systems	Cat# MLA00
Mouse IL-6 Quantikine ELISA Kit	R&D Systems	Cat# M6000B
Mouse LIF Quantikine ELISA Kit	R&D Systems	Cat# MLF00
Mouse GM-CSF Quantikine ELISA Kit	R&D Systems	Cat# MGM00
RNeasy Kit for RNA isolation	QIAGEN	Cat# 74104
RevertAid First Strand cDNA Synthesis Kit	Thermo Fisher Scientific	Cat# K1622
Membrane and Cytosol Protein Extraction Kit	Beyotime Biotech Inc	Cat# P0033
Nuclear and Cytoplasmic Protein Extraction Kit	Beyotime Biotech Inc	Cat# P0027
EZ-Magna ChIP™ A/G Chromatin Immunoprecipitation Kit	Millipore	Cat# 17-10086

(Continued on next page)

**Continued**

REAGENT or RESOURCE	SOURCE	IDENTIFIER
Pierce™ BCA Protein Assay Kits	Thermo Fisher Scientific	Cat# A65453
Hyperactive Universal CUT&Tag Assay Kit	Vazyme	Cat# TD903
Sircol Collagen Assay Kit	Biocolor Assays	Cat# S5000
Duo-Lite Luciferase Assay System	Vazyme	Cat# DD1205

**Deposited data**

RNA Sequencing data	This paper	GEO: GSE267820
Cut-tag Sequencing data	This paper	GEO: GSE264148
Multimodal Mapping of the Tumor and Peripheral Blood Immune Landscape in Human Pancreatic Cancer	NCBI Gene Expression Omnibus	GEO: GSE155698
Single-Cell RNA-seq Highlights Intra-tumoral Heterogeneity and Malignant Progression in Pancreatic Ductal Adenocarcinoma	Genome Sequence Archive	PRJCA001063

**Experimental models: Cell lines**

Panc1	ATCC	Cat# CRL-1469; RRID: CVCL_0480
Capan2	ATCC	Cat# HTB-80; RRID: CVCL_0026
AsPC-1	ATCC	Cat# CRL-1682; RRID: CVCL_0152
HPAC	ATCC	Cat# CRL-2119; RRID: CVCL_3517
Mouse PDAC cell lines: 399, 921, and 1050	Ref. <sup>39</sup>	N/A
Mouse PSCs	This paper	N/A
Human PDAC CAFs	This paper	N/A
Human PDAC organoids	Dr. Maximilian Reichert, Department of Medicine II, Klinikum rechts der Isar, Technische Universität München	N/A
Mouse PDAC organoids	This paper	N/A

**Experimental models: Organisms/strains**

<i>Ptfl1</i> <sup>Cre/+</sup> ( <i>p48</i> <sup>Cre/+</sup> )	Jens T. Siveke, Division of Solid Tumor Translational Oncology, University Hospital Essen, Germany	N/A
<i>Agr2</i> <sup>flox/flox</sup>	EMMA	Strain #EM:04307; RRID: IMSR_EM:04307
LSL-RosaCAG- <i>Agr2</i>	Cyagen Biosciences	N/A
C57BL/6J	Charles River	Strain #213
BALB/c Nude	Charles River	Strain #401
<i>Ptfl1</i> <sup>CreERTM/+</sup>	Jackson Laboratory	Strain #019378; RRID: IMSR_JAX:019378
<i>p53</i> <sup>flox/flox</sup>	Jackson Laboratory	Strain #008462; RRID: IMSR_JAX:008462
Loxp-STOP-Loxp <i>Kras</i> <sup>G12D</sup> (LSL- <i>Kras</i> <sup>G12D</sup> )	Jackson Laboratory	Strain #008179; RRID: IMSR_JAX:008179

**Oligonucleotides**

Primers for real-time PCR analysis, see methods details	This paper	N/A
Primers for CHIP PCR analysis, see methods details	This paper	N/A
Human AGR2 sgRNA, see methods details	GENECHEM	N/A
Human β-Catenin shRNA, see methods details	GENECHEM	N/A
Human c-JUN siRNA, see methods details	HANBIO	N/A

**Recombinant DNA**

AGR2 <sup>WT</sup> expression vector	OriGene Technologies	Cat# RC202023
AGR2 <sup>ΔNLS</sup> expression vector	GENECHEM	N/A
AGR2 <sup>ΔSP</sup> expression vector	GENECHEM	N/A

(Continued on next page)

**Continued**

REAGENT or RESOURCE	SOURCE	IDENTIFIER
AGR2 <sup>CB1A</sup> expression vector	GENECHEM	N/A
GV354 luciferase vector	GENECHEM	N/A
GV715 luciferase vector	GENECHEM	N/A
<b>Software and algorithms</b>		
GraphPad Prism V.7	GraphPad Software	<a href="https://www.graphpad.com/">https://www.graphpad.com/</a>
IBM SPSS V.27	IBM	<a href="https://www.ibm.com/spss">https://www.ibm.com/spss</a>
Integrative Genomics Viewer	IGV	<a href="https://igv.org">https://igv.org</a>
R statistical software version 4.1.2	The R Project	<a href="https://www.r-project.org">https://www.r-project.org</a>
DESeq2	Bioconductor	<a href="https://bioconductor.org/packages/release/bioc/html/DESeq2.html">https://bioconductor.org/packages/release/bioc/html/DESeq2.html</a>
Rsubread	Bioconductor	<a href="https://bioconductor.org/packages/release/bioc/html/Rsubread.html">https://bioconductor.org/packages/release/bioc/html/Rsubread.html</a>
HISAT2	The University of Texas Southwestern Medical Center	<a href="https://daehwankimlab.github.io/hisat2">https://daehwankimlab.github.io/hisat2</a>
Bowtie 2 v2.5.4	SourceForge	<a href="https://bowtie-bio.sourceforge.net/bowtie2">https://bowtie-bio.sourceforge.net/bowtie2</a>
Seurat v4.0	Seurat	<a href="https://satijalab.org/seurat">https://satijalab.org/seurat</a>
Harmony v1.0	Harmony	<a href="https://portals.broadinstitute.org/harmony">https://portals.broadinstitute.org/harmony</a>
<b>Other</b>		
Gallios flow cytometer	Beckman Coulter, USA	N/A
Agilent Bioanalyzer 4150	Agilent Technologies, CA, USA	N/A
Novaseq 6000 Sequencer	Illumina, San Diego, CA USA	N/A

**EXPERIMENTAL MODEL AND STUDY PARTICIPANT DETAILS**

**Patient material and tissues**

We obtained 99 PDAC tissues for immunohistochemistry analysis of AGR2 from patients who underwent pancreatic resections at Department of Surgery, Klinikum rechts der Isar. All sample diagnoses were confirmed histologically. The cohort included 58 males and 41 females, with a mean age of 65.46 years (range: 44–86 years). Samples were processed by either snap-freezing in liquid nitrogen or fixation in paraformaldehyde solution for 24 h, followed by paraffin embedding for histological analysis. In addition, serum samples were obtained for AGR2 and IGF1 measurements from 172 PDAC patients (108 males and 64 females, mean age: 62.60 years, range: 41–91 years) from Klinikum rechts der Isar, the First Affiliated Hospital of Nanjing Medical University, and Nanjing Drum Tower Hospital for enzyme-linked immunosorbent assay (ELISA) analysis. For a subset of patients, matched tissue samples and serum samples were used for immunohistochemical staining of tumor microenvironment markers. Comprehensive clinical and pathological data were collected for all patients. The use of tissue and serum samples was approved by the local ethics committee (approval number: 80/17S and 409/19S-SR), and written informed consent was obtained from patients before surgery (Department of Surgery, Klinikum rechts der Isar, Technical University Munich). In addition, this study was also approved by the local ethics committee of Ulm University Hospital (approval number: 264/21, Department of Surgery, Ulm University) and University Hospital of Heidelberg (approval number: S-035/2024, Department of General, Visceral and Transplantation Surgery, University of Heidelberg), and the Nanjing Drum Tower Hospital (approval number: 2021-423-01).

**Transgenic mice**

Mouse breeding was conducted at a specific pathogen-free (SPF) mouse facility at the Technical University of Munich. The pancreas-specific Cre recombinase line *Ptf1α*<sup>Cre/+</sup> (also known as *p48*<sup>Cre/+</sup>) was a generous gift from Prof. Dr. Jens T. Siveke (Division of Solid Tumor Translational Oncology, University Hospital Essen, Germany). The inducible Cre recombinase line specific to the pancreas (*Ptf1a*<sup>CreERTM</sup>), *Loxp-STOP-Loxp-Kras*<sup>G12D</sup> (LSL-*Kras*<sup>G12D</sup>) line and the *p53*<sup>flox/flox</sup> line were all acquired from Jackson Laboratory (Bar Harbor, USA). The *Agr2*<sup>flox/flox</sup> line was acquired from EMMA (Munich, Germany), while mice with *LSL-Rosa*<sup>CAG-Agr2</sup> were obtained from Cyagen Biosciences (Santa Clara, USA). Wild-type (C57BL/6J) mice were obtained from Charles River (Sulzfeld, Germany). All mouse experiments complied with the German Federal Animal Protection Laws and were approved by the Institutional Animal Care and Use Committees of the government of Bavaria and the Technical University of Munich under reference number 55.2-1-54-2532-197-2016. To induce *Ptf1α* Cre<sup>ERT</sup> activity, 4 mg/20 g body weight tamoxifen (T564, Sigma-Aldrich, Steinheim, Germany) was orally gavaged every 48 h three times at 5 weeks of age. Acute pancreatitis in 8-week-old transgenic mice was induced by administering caerulein as previously reported.<sup>18</sup> Briefly, caerulein treatment (Sigma Aldrich, C9026) was administered via eight

hourly intraperitoneal injections (20  $\mu$ g/mL, 100  $\mu$ L per injection) over two consecutive days, whereas control mice received injections of 0.9% NaCl solution under the same schedule.

### **In vivo transplantation assays**

Male BALB/c nu/nu athymic mice (CAnN.Cg-Foxn1nu/Crl) at 6 weeks of age were used to establish subcutaneous models via subcutaneous injection. Briefly, mice were anesthetized using isoflurane and  $1 \times 10^6$  cells resuspended with 50  $\mu$ L of Matrigel were injected into the subcutaneous space of the left flanks. Four weeks after injection, the mice were euthanized, and the tumor tissues were collected and photographed. Subsequently, the tissues were fixed and subjected to the next step of pathological staining. The study was approved by the Ethics Review Committee for Animal Experimentation at Nanjing Drum Tower Hospital under reference number 2020AE01088.

### **Treatment of KPC mice**

Both male and female *Ptf1 $\alpha$ <sup>CreERTM</sup>; LSL\_Kras<sup>G12D/+</sup>; p53<sup>fllox/fllox</sup>* (KPC) mice were treated with tamoxifen and caerulein at five weeks and eight weeks of age. Five weeks after caerulein injection, when a tumor can be touched, KPC mice were assigned to a treatment group: control, PPP, Agr2-Ab, or PPP and Agr2-Ab combination. PPP was administered as an oil solution at 20 mg/kg by intraperitoneal injection three times per week, and Agr2-Ab was administered at 4 mg/kg by intraperitoneal injection three times per week. Mice were euthanized after 17 days of treatment and the tumor volume was measured.

### **Cell lines and culture**

The PDAC cell lines Panc1, Capan2, AsPC-1, and HPAC were purchased from ATCC (Beijing, China). Murine PDAC cell lines including 399, 921, and 1050 were isolated from the PDAC tissues of *p48<sup>Cre/+</sup>; Kras<sup>G12D/+</sup>; Tsc1<sup>-/+</sup>* mice, as previously described.<sup>39</sup> All cells were cultured in DMEM medium (Gibco/Thermo Fisher Scientific, Darmstadt, Germany) containing 10% FBS (Gemini Bio Products, West Sacramento, CA, US) and 1% penicillin/streptomycin (Gibco). All cell lines were tested negative for mycoplasma every month using the MycoProbe Mycoplasma Detection Kit (R&D Systems, Minneapolis, USA). STR analysis for human cell line authentication was performed by GENEWIZ (Suzhou, China).

## **METHOD DETAILS**

### **AAV vector production and transduction**

Adeno-associated viruses (AAV) of serotype 8 for overexpression of *Agr2<sup>WT</sup>* (AAV8-*Agr2<sup>WT</sup>*) and *Agr2<sup>ΔSP</sup>* (AAV8-*Agr2<sup>ΔSP</sup>*) were produced by GENECHM (Shanghai, China) within frame of custom service. The coding sequence of the wildtype *Agr2* gene (*Agr2<sup>WT</sup>*, GenBank accession number: NM\_011783), as well as the *Agr2* variant lacking the signal peptide (*Agr2<sup>ΔSP</sup>*), were amplified and subsequently cloned into the GV331 vector plasmid (CMV promoter-driven *Agr2<sup>WT</sup>/Agr2<sup>ΔSP</sup>* fused to EGFP, followed by the SV40 polyA signal) using the *AfeI* restriction enzyme. A plasmid devoid of the *Agr2* coding sequence was used as the control. In 5-week-old *p48<sup>Cre/+</sup>; LSL-Kras<sup>G12D/+</sup>* (KC) mice, we conducted AAV-mediated gene transfer via intrapancreatic injection, targeting three sites in the pancreas of each mouse with an injection volume of  $5 \times 10^{12}$  viral particles per site. Three weeks post-injection, the mice were euthanized, and their pancreata and plasma were collected.

### **Human and mouse PDAC-derived organoid isolation and passage**

Human PDAC-derived organoids were provided by Dr. Maximilian Reichert (Department of Medicine II, Klinikum rechts der Isar, Technische Universität München). The protocol of isolation and passaging is described in our previous study.<sup>18</sup> Mouse PDAC-derived organoids were isolated from KPC mice. In brief, the mice were euthanized and the tissue were minced into pieces of roughly 0.5 mm<sup>3</sup>. Then the tissues were digested with collagenase II in DMEM/F12 for 45 min at 37°C. After washing, the cells were resuspended using basement matrix (Corning, New York, USA), seeded in 24-well plates and incubated for 5–10 min at 37°C or until the basement matrix is solidified.

### **Isolation of human CAFs**

Human primary CAFs were isolated from PDAC tissues by the outgrowth method as previously described.<sup>40</sup> Briefly, PDAC tissues were obtained during surgery from patients with untreated resectable PDAC, and then minced into small pieces (0.5–1 mm<sup>3</sup>) and cultured in DMEM/F12 supplemented with 10% FBS and 1% penicillin-streptomycin. After approximately 2 weeks, fibroblasts migrated from the fragments of the tissue, were trypsinized and transferred to culture flasks for expansion. The isolated cells were confirmed to be CAFs by detecting markers of pan-fibroblast (COL1A1, COL1A2 and PDPN) and macrophages (CD68) by RT-PCR, and by detecting *KRAS* Exon2 by sanger sequencing to rule out carrying *KRAS* mutations. AsPC-1 cells were used as control for these tests. All functional assays of CAFs were performed before passage 6.

### **Isolation of mouse PSCs**

Mouse PSCs were isolated from the murine pancreas by the density gradient method as described.<sup>41</sup> Briefly, C57BL/6 mice were euthanized and the pancreatic tissue was separated and cut into small pieces, and placed in a digestive solution (0.05% collagenase

P, 0.1% DNase I, GBSS buffer) for digestion for 30 min. The digested tissue was filtered through a 100  $\mu$ m strainer, washed, centrifuged to obtain cell pellets, and then resuspended in 47.5% Histoden Z. The top solution (GBSS buffer containing 0.3% BSA) was carefully added to the upper layer of the resuspension, and then centrifuged with slowly switched off. Cells were harvested from the fuzzy band in the middle layer, washed and cultured in DMEM/F12 supplemented with 10% FBS and 1% penicillin-streptomycin.

### Co-culture of tumor organoids and CAFs/PSCs

PSCs or CAFs at a concentration of  $1 \times 10^5$  were seeded in Matrigel on top of the *trans*-well membrane with organoids growing in the lower compartment in 24-well plates. After starvation with serum-free DMEM for 12 h, PSCs or CAFs in the upper chamber were co-cultured with the organoids below. AGR2 antibodies and picropodophyllin (PPP, Cat# S7668, Selleck, München, Germany) were added to the co-culture system. The morphology of the organoids was photographed and collected in 5 random fields of view at 24, 48, 72, and 96 h of co-culture, and the area occupied by the organoids in each field was measured. After 48 h of co-culture, RNA was extracted from the CAFs/PSCs in the upper chamber for RT-PCR analysis, proteins were extracted from the organoids in the lower chamber for immunoblotting analysis, and the culture medium was collected for ELISA analysis.

### AGR2 knockout cell lines

To achieve knockout of AGR2 in Panc1, Capan2, AsPC-1 and HPAC cells, lentiviral CRISPR/Cas9 was purchased from GENECHM (Shanghai, China) and were then infected into PDAC cells. The gRNA sequences targeting AGR2 were 1st-CTTGATGATTATTCATCACT; 2nd-CTCTATATAAATCCAAGACA. In brief, PDAC cells were cultured at 60% confluence in a 6-well plate, transfected with lentivirus, and selected with puromycin (Sigma Aldrich, P8032). Subsequently, single clone cell lines with AGR2 knockout were obtained using a limited dilution method.

### shRNA and siRNA knockdown studies

To silence endogenous c-JUN and  $\beta$ -Catenin expression in PDAC cells or CAFs, we utilized siRNA targeting human c-JUN provided by HANBIO (Shanghai, China) and lentivirus producing shRNA targeting human  $\beta$ -Catenin mRNA provided by GENECHM (Shanghai, China) with the hU6-MCS-CMV-Puromycin as the viral vector. The siRNA targeting c-JUN was 5'-GCAAACCUCAGCAA CUUCATT-3'. The sequences targeted by the shRNA for  $\beta$ -Catenin were as follows: sh- $\beta$ -Catenin#1, 5'-GCTTGGAAATGAGACTGCTGAT-3', sh- $\beta$ -Catenin#2, 5'-AGGTGCTATCTGTCTGCTCTA-3', sh- $\beta$ -Catenin#3, 5'-CCATTGTTGTGCAGCTGCTT-3'. In summary, PDAC cells or human CAFs were seeded in a 6-well plate at 60% confluence. After 24 h, the cells were transduced with a multiplicity of infection (MOI) of 100. To establish stably transfected cells, cells were continuously cultured with 2  $\mu$ g/mL puromycin. The efficiency of gene knockdown was assessed using qRT-PCR and Western blot.

### Plasmid generation

Human wild-type AGR2 expression vector (AGR2<sup>WT</sup>, RC20223) was purchased from OriGene Technologies (Beijing, China). And AGR2 <sup>$\Delta$ NLS</sup>, AGR2 <sup>$\Delta$ SP</sup> and AGR2<sup>C81A</sup> were generated by GENECHM (Shanghai, China) based on the wild-type vector as our previous study described.<sup>18</sup> In order to prevent overexpression of AGR2 in AGR2-knockout PDAC cells from being recognized by sgRNA, we performed synonymous mutations on the recognition site of sgRNA#1.

### ELISA assay

The concentrations of cytokines in culture media or human/mouse serum were detected using Quantikine ELISA kits (R&D Systems, Minneapolis, US) directed toward human IGF-1 (#DG100B) and human AGR2 (#NBP2-78743), and toward mouse IGF-1 (#MG100), IL-1 $\alpha$  (#MLA00), IL-6 (#M6000B), LIF (#MLF00) and GM-CSF (#MGM00) according to the manufacturer's instructions.

### Western blot

Total protein was extracted using RIPA Lysis, and subcellular fractions protein was extracted as mentioned above. Equivalent amounts of protein were separated by SDS-PAGE and transferred to PVDF membranes. Then the membranes were incubated with primary antibodies and secondary antibodies labeled with horseradish peroxidase, visualized using Immobilon ECL Ultra Western HRP Substrate (#WBULP-100ML, Millipore/Merck, Darmstadt, Germany).

### Flow cytometry analysis

To detect the distribution of IGF1R on the cell membrane surface, flow cytometry was performed. Briefly, AGR2 knockout and control pancreatic cancer cells were trypsinized, harvested and incubated with IGF1R antibody or IgG antibody. Goat anti-rabbit Alexa Fluor 488 was used for further fluorescent labeling, and cells were then detected by flow cytometry. To determine the effect of rAGR2 on the proliferation of CAFs, CytoTrackTM Red (Bio-Rad, Minneapolis, USA) was used to label the CAFs with or without rAGR2 treatment for 24 h (500 ng/mL). Flow cytometry analysis was performed using a Gallios flow cytometer (Beckman Coulter, USA).

### Luciferase reporter assay

Reporter plasmids with different lengths of the AGR2 promoter (position-2988~+12, -2160~+12, -1988~+12-1068~+12 relative to the transcription initiation site) were constructed and cloned into the GV354 luciferase vector in GENECHM (Shanghai, China),

which expresses both the firefly and renilla luciferase gene. Additional mutant of the –1068~+12 construct of the AGR2 promoter was also generated (position-384~–397). Additionally, reporter plasmids for the wildtype and mutant (position-1611~–1625, –1437~–1451, –1063~–1077, –1026~–1040, –861~–875 and –662~–676 relative to the transcription initiation site) IGF1 promoter were constructed and cloned into the GV715 luciferase vector, also provided by GENECHM (Shanghai, China), which specifically expresses the firefly luciferase gene. All constructs were validated through sequencing. PDAC cells or CAFs were seeded in a 24-well plate and transfected 24 h later using Lipofectamine 3000 with 100 ng of the reporter construct, or an empty vector (GV354 or GV715) as a negative control. Following treatment, luciferase activity was assessed using the Duo-Lite Luciferase Assay System (#DD1205, Vazyme, Nanjing, China).

### Immunohistochemistry and immunofluorescence staining of tissue

Mice and human tissues were fixed in 4% paraformaldehyde (PFA) for 24 h, then embedded in paraffin and sliced into sections with a thickness of 2  $\mu$ m. The tissue sections were subjected to a heat treatment at 60°C for 1 h, followed by deparaffinization in roti-clear solution and rehydration in a series of ethanol solutions. Antigen retrieval was carried out using either citrate buffer (pH 6.0; 10 mM citric acid; 0.05% Tween 20) or Tris/EDTA (pH 9.0; 10 mM Tris; 1 mM EDTA; 0.05% Tween 20) in a microwave oven for 15 min. To block endogenous peroxidases, the sections were incubated in 3% hydrogen peroxide, and nonspecific reactivity was blocked using 10% goat serum. Subsequently, the sections were incubated with the primary antibody overnight at 4°C. For immunohistochemistry (IHC), the sections were then incubated with horseradish peroxidase-linked secondary antibodies against rabbit or mouse for 1 h at room temperature, followed by a color reaction using diaminobenzidine and counterstaining with hematoxylin. The sections were dehydrated and mounted after this process. For immunofluorescence (IF) staining, the sections were incubated with fluorescence-labeled secondary antibodies for 1 h at room temperature and mounted using a mounting medium containing DAPI. For quantitative IHC staining, we used H-Scores to calculate stromal-related staining ( $\alpha$ -SMA, PDPN, IL-6 and Sirius Red). Briefly, the staining intensity (ranked from 0 to 3) and staining area (percentage) were evaluated separately, and then the two were multiplied to obtain H-scores. For IHC assessment of immune cells (CD3, CD4, CD8, FOXP3, CD68, CD206, CD20, B220 and F4/80), the numbers of positive cells/mm<sup>2</sup> were calculated.

### If staining of cells

The cells were seeded in glass bottom dishes (#150680, Thermo Fisher Scientific, Darmstadt, Germany) at approximately 60% confluence. Once the cells adhered to the dish, they were fixed with 4% PFA and washed with PBS. Subsequently, the cells were permeabilized with 0.1% Triton X-100 and blocked in 10% FBS for 2 h. Following this, the cells were incubated with primary antibodies at 4°C overnight, and then with secondary antibodies and DAPI for 1 h at room temperature. Finally, cells were visualized by a fluorescence microscope (Olympus, Tokyo, Japan).

### qRT-PCR

Total RNA from cells or organoids is isolated using RNeasy Kit (#74104, QIAGEN, Hilden, Germany), and cDNA was synthesized using RevertAid First Strand cDNA Synthesis Kit (#K1622, Thermo Fisher Scientific, Darmstadt, Germany) according to the manufacturer's instructions. Then, SYBR Green Master Mix (#A46110, Applied Biosystems/Thermo Fisher Scientific) was applied for two-step real-time RT-PCR analysis using the LightCyclerTM480 system. The results were quantified using the 2<sup>(delta)(delta)</sup>CT method with housekeeping gene Gapdh as the control gene for internal normalization. Primers list: *IGF1R* (forward: 5'-AGTATGGAGGGGC-CAAGCTA-3'; reverse: 5'-CCTGTTTTGGCCTGGACATAG-3'), *AGR2* (forward: 5'-TCAACTCTGGCCAGGAATC-3'; reverse: 5'-TACTTTGCCAGAGGCTTTCCC-3'), *IGF1* (forward: 5'-TTTCAACAAGCCCACAGGGT-3'; reverse: 5'-TTGAGGGGTGCGCAATA CAT-3'), *IL-6* (forward: 5'-ACTCACCTTCAGAACGAATTG-3'; reverse: 5'-CCATCTTTGGAAGGTTGAGTTG-3'), *CFD* (forward: 5'-GACAGCTGCAAGGGTGACTC-3'; reverse: 5'-GCTTCTTGCGGTTGCCG-3'), *CCL2* (forward: 5'-CATGAAAGTCTCTGCCGCC-3'; reverse: 5'-GGGCATTGATTGCATCTGGCT-3'), *MYL9* (forward: 5'-GCTCGGCTGAAACTCCTCAT-3'; reverse: 5'-CCTTATGA CCCTGGTGTCCG-3'), *ACTA2* (forward: 5'-GAGGGAAGGTCTTAACAGCC-3'; reverse: 5'-GTCCCGGGGATAGGCAAAGT-3'), *CTGF* (forward: 5'-ACCGACTGGAAGACACGTTTTG-3'; reverse: 5'-CCAGGTTCAGCTTCGCAAGG-3'), *GAPDH* (forward: 5'-TCCAAA ATCAAGTGGGGCGA-3'; reverse: 5'-AAATGAGCCCCAGCCTTCTC-3'), *Igf1* (forward: 5'-CTGGACCAGAGACCCTTTGC-3'; reverse: 5'-GGACGGGGACTTCTGAGTCTT-3'), *Il-1 $\alpha$*  (forward: 5'-AGGGAGTCAACTCATTGGCG-3'; reverse: 5'-ACTTCTGCCTGACGAGCTTC-3'), *Il-6* (forward: 5'-CTGCAAGAGACTTCCATCCAGTT-3'; reverse: 5'-GAAGTAGGGAAGGCCGTGG-3'), *Lif* (forward: 5'-AACT GGCACAGCTCAATGG-3'; reverse: 5'-AGGCGCACATAGCTTTTCC-3'), *Ctgf* (forward: 5'-TGTACGGAGACATGGCGTAA-3'; reverse: 5'-GTGGGATAGTTCTCCACG-3'), *Tgf- $\beta$ 1* (forward: 5'-GCCTGAGTGGCTGTCTTTTG-3'; reverse: 5'-GGGGCTGATCCCCTTGA TTT-3'), *Acta2* (forward: 5'-TGCAGAAGACCTGGCCTCTA-3'; reverse: 5'-GTGCCAGCAAAGGTCAGAGA-3'), *Gapdh* (forward: 5'-AGGTCGGTGTGAACGGATTG-3'; reverse: 5'-TGTAGACCATGTAGTTGAGGTCA-3').

### Protein extraction from subcellular fractions

The nuclear and cytoplasmic extraction from CAFs was performed using the Nuclear and Cytoplasmic Protein Extraction Kit (#P0027, Beyotime, Shanghai, China). The membrane and cytosol extraction from PDAC cells was performed using the Membrane and Cytosol Protein Extraction Kit (#P0033, Beyotime Biotech Inc, Jiangsu, China). Subsequently, immunoblot analysis was carried out using the protein extracted from subcellular fractions.

### Chromatin immunoprecipitation (CHIP) qPCR

Control or IGF1-treated Panc1 or Capan2 cells ( $1 \times 10^6$ ) each were used for CHIP assays using the EZ-Magna ChIP A/G Chromatin Immunoprecipitation Kit (#17-10086, Millipore, Darmstadt, Germany) following instructions provided by the manufacturer. Anti-IgG and anti-c-JUN antibodies were used to immunoprecipitate chromosome fragments. The immunoprecipitated DNA was used as a template for qPCR. The primers sequences are available as follows: forward: 5'-CTGTGCCAGCTCTAGCCAAA-3'; reverse: 5'-GGTGGGATTGAGGTATGCCC-3'.

### Co-immunoprecipitation

For co-IP, tissues or cells were lysed in Pierce IP lysis buffer (#87787, ThermoFisher Scientific, Darmstadt, Germany) containing protease and phosphatase inhibitors. The lysates were then centrifuged at 12,000x rpm for 15 min. Protein concentrations were determined using a BCA kit (#A65453, Thermo Fisher Scientific), and equal amounts of protein were incubated with specific antibody overnight at 4°C with rotation. Afterward, 100  $\mu$ L of pre-washed Pierce Protein A/G Agarose (#20421, ThermoFisher Scientific) were added and further incubated with rotation for 2 h at room temperature. The beads were then washed five times with 0.5mL of IP Buffer, and SDS loading buffer was added to the samples. Following a 10-min incubation at 95°C, the samples were subjected to SDS-PAGE and subsequently analyzed by Western blot.

### Transwell assay

For transwell analysis, 50,000 CAFs resuspended in serum-free DMEM were seeded in the upper chamber and DMEM medium with 20% FBS was added in the bottom chamber. After culture for 24 h, cells were fixed with 4% paraformaldehyde and stained with 1% crystal violet. Cells were imaged and counted using a microscope and a 20 $\times$  magnification.

### RNA sequencing

For RNA sequencing of PDAC cells (Capan2 and Panc1) and human CAFs total RNA was extracted from PDAC cells and CAFs using the RNeasy Kit (#74104, QIAGEN, Darmstadt, Germany) and RNA integrity was assessed using an Agilent Bioanalyzer 4150 (Agilent Technologies, CA, USA). Only qualified samples were used for library construction. Paired-end libraries were prepared and sequenced on a Novaseq 6000 sequencer (Illumina, San Diego, CA, USA), generating 150 bp paired-end reads. Clean reads were aligned to the reference genome with HISAT2 in orientation mode, and FeatureCounts was used for read counting per gene. FPKM was calculated based on gene length and mapped read count. Differential expression analysis was performed using DESeq2, defining significantly differentially expressed genes as those with  $|\log_2FC| > 1$  and  $P_{adj} < 0.05$ .

### Cut&Tag sequencing

Control or IGF1-treated Panc1 cells at a concentration of  $5 \times 10^4$  were submitted for Cut&Tag analysis. c-JUN antibody was used to purify DNA fragments that bind to c-JUN. Libraries were constructed using the Hyperactive Universal CUT&Tag Assay Kit from Illumina (#TD903, Vazyme, Nanjing, China) according to the manufacturer's protocol and sequenced on an Illumina NovaSeq6000 platform in paired-end reads. Paired-end reads were aligned with *Homo sapiens*. GRCh38 genome using Bowtie2. Mapped reads were visualized using the Integrative Genomics Viewer (IGV).

### Detection of collagen in culture medium

The Sircol Collagen Assay Kit (#S5000, Biocolor Assays, Carrickfergus, UK) was used to detect the collagen concentration in culture medium according to the manufacturer's protocol.

### Construction of AGR2 neutralizing antibody

The construction process of monoclonal AGR2-neutralizing antibodies took place at Abcam (Shanghai, China). In brief, rabbit Fc-tagged AGR2 protein was expressed in HEK293T cells and purified. The purified AGR2 protein was then used for the immunization of three rabbits, with each rabbit receiving 4–5 injections. Subsequently, splenectomies were performed to isolate lymphocytes, enriching for B cells with antigen-specificity. B-cell fusion and clone selection were carried out using the "straight to clone" method. The supernatant of hybridoma cells was utilized for antigen binding selection based on ELISA and Western blot methods to obtain the most specific clones, followed by sequencing of these cloned cells. Then, the synthesis of variable heavy and variable light chain DNA was performed, and the cDNA was cloned into a commercially available human Fc vector (human IgG1). The expression construct was validated by testing the expressions of the recombinant antibody. To obtain AGR2 monoclonal neutralizing antibodies, production and purification of the clone were expanded.

### Single cell data analysis

We analyzed single-cell RNA-seq data using R statistical software (version 4.1.2, Vienna, Austria) along with the Seurat v4.0 and Harmony v1.0 toolkits. The datasets were obtained from GEO: GSE155698 in the Gene Expression Omnibus (GEO) and PRJCA001063 in the Genome Sequence Archive (GSA), both publicly available. We filtered out cells with fewer than 200 genes detected or mitochondrial gene expression above 10% and genes detected in <3 cells were also eliminated. The original data was then normalized using the LogNormalize function (features = 3,000) and the Harmony function (max.iter.harmony = 20) from the Seurat package.

Dimensionality reduction was performed using principal component analysis (PCA), and the resulting data were visualized using Uniform Manifold Approximation and Projection (UMAP) with the Seurat package in R. To identify distinct cell populations, we utilized the FindClusters function within the Seurat package, applying a graph-based clustering algorithm with a resolution parameter set between 0.05 and 0.25. For visualization of candidate genes, dot plots and violin plots were generated using the dotplot function and the VlnPlot function, respectively, from the Seurat package. Lastly, we used a volcano plot to illustrate the differential expression of significant genes between IGF1-positive and negative cells.

### QUANTIFICATION AND STATISTICAL ANALYSIS

Statistical analyses were performed using either GraphPad Prism V.7 software (GraphPad, San Diego, CA, USA) or IBM SPSS V.27 software (IBM, New York, USA). The data are reported as means  $\pm$  standard deviation (s.d.), and significant differences were determined using the unpaired Student's *t* test, one-way analysis of variance (ANOVA), or Pearson's chi-square test. Kaplan-Meier survival analysis was employed for all survival studies, with group comparisons made using the log-rank test. A *p* value  $<0.05$  was considered as statistically significant. For animal studies, the sample size was predetermined by our prior experiments. Statistical details of experiments were described in Figure Legends.